A8 B16

RM No. A8B16

NACA RM No. A8B16

NACA

RESEARCH MEMORANDUM

AN EXPERIMENTAL INVESTIGATION OF NACA SUBMERGED INLETS AT HIGH SUBSONIC SPEEDS. I - INLETS FORWARD OF THE WING LEADING EDGE

By Charles F. Hall and F. Dorn Barclay

Ames Aeronautical Laboratory
Moffett Field, Calif.

NATIONAL ADVISORY COMMITTEE
FOR AERONAUTICS

WASHINGTON

June 9, 1948

NATIONAL ADVISORY COMMITTEE FOR AERONAUTICS

RESEARCH MEMORANDUM

AN EXPERIMENTAL INVESTIGATION OF NACA SUBMERGED INLETS AT HIGH SUBSONIC SPEEDS. I – INLETS FORWARD OF THE WING LEADING EDGE

By Charles F. Hall and F. Dorn Barclay

SUMMARY

This report covers the first part of an experimental investigation of NACA submerged inlets at four locations on the fuselage of a fighter airplane model for Mach numbers from 0.30 to 0.875. Data are presented showing the characteristics of the model without inlets and with inlets 16.7 percent of the root chord forward of the wing-root leading edge and equipped with small boundary-layer deflectors.

The data show that variations in the mass of air entering the inlet had a large effect on the ram-recovery ratio. Representative values of ram-recovery ratio were 0.50 with zero flow, 0.90 with 0.6 mass-flow coefficient, and 0.95 with 1.00 mass-flow coefficient. Variations in Mach number and angle of attack, in general, caused less than a 0.03 variation in the ram-recovery ratio.

INTRODUCTION

An experimental development of submerged inlets was conducted at the Ames Aeronautical Laboratory in a small wind channel. (See references 1 and 2.) The NACA submerged inlet, which had very good pressure-recovery characteristics, was evolved during this development. The investigation was made at a low Mach number with the inlet built into the wall of the channel. In order to extend the investigation to high subsonic Mach numbers and to determine the characteristics of the submerged inlet on a model, the research program discussed in the present report was conducted.

In the present tests, attention was concentrated on the inlet found to have the most satisfactory pressure-recovery characteristics from the tests of reference 1. For this inlet, the effects of the

following model variations were investigated:

1. Inlet location with respect to the wing and fuselage
2. Boundary-layer thickness on the fuselage
3. Boundary-layer deflectors
4. Inlet lip angle

Because of the large number of data obtained and the time required to analyze them, several reports will be issued covering this program. In this, the first report, the characteristics of the model without inlets and with inlets 16.7 percent of the root chord forward of the wing leading edge are presented.

The investigation was conducted in the Ames 16-foot high-speed wind tunnel at the request of the Bureau of Aeronautics, Navy Department. In conjunction with the program conducted in the Ames 16-foot wind tunnel, an investigation of the characteristics of several types of submerged inlets on a fighter airplane model similar to that used in the 16-foot wind tunnel but designed for a prop-jet power unit was made in one of the Ames 7- by 10-foot wind tunnels. The results of the first part of that investigation have been reported in reference 3.

SYMBOLS

The symbols used in this report and their definitions are as follows:

α_u angle of attack uncorrected for tunnel-wall effects, degrees (The angle is measured relative to the fuselage reference line.)

M Mach number (V/a)

P pressure coefficient $[(p-p_o)/q_o]$

P_{cr} critical pressure coefficient (the pressure coefficient at which the speed of sound is reached)

p static pressure, pounds per square foot

H effective total pressure, pounds per square foot

H' total pressure at a point, pounds per square foot

C_D drag coefficient $\left(\frac{\text{drag}}{q_o S}\right)$

m mass flow (ρAV), slugs per second

m_o the mass of fluid in the free stream passing through an area equal to the entrance area of the inlet ($\rho_o A_1 V_o$), slugs per second

ρ density of air, slugs per cubic foot

A cross-sectional area of duct, square feet

V speed of air stream, feet per second

q dynamic pressure, pounds per square foot

S wing area, square feet

a speed of sound in stream, feet per second

E energy, foot-pounds per second

Δs entropy change, Btu per degree Fahrenheit

γ ratio of specific heat at constant pressure to that at constant volume

c_p specific heat at constant pressure, Btu per pound per degree Fahrenheit

T absolute stagnation temperature, degrees Fahrenheit

T' absolute stagnation temperature at a point, degrees Fahrenheit

Subscripts:

o free stream

1 entrance of inlet

s stagnation

APPARATUS

In the present investigation a model of a typical high-speed fighter airplane was used. A picture of the model with the NACA

submerged inlets forward of the wing leading edge is shown in figure 1. Figure 2 is a drawing showing all the inlet locations investigated and giving dimensional data for the model. The fuselage stations used in the figure and throughout the report are in inches from the fuselage nose. Water lines (W.L.) are in inches above or below the fuselage reference line. For simplicity, an empennage was not built on the model.

Dimensional data for the ramp, lip, and boundary-layer deflectors used during the investigation are shown in figure 3. For all locations of the inlet, the ramp angle (7°) and ramp length (21.10 in.) remained constant. The curvature at the beginning of the ramp was different at the various locations, however, due to the difference in fuselage shape at the various ramp locations.

Behind the inlet, the induction system consisted of a duct having a cross-sectional area equal to the entrance area, which led to a diffuser. Since the location of the diffuser remained fixed throughout the tests, the length of the constant-area duct depended on the inlet location. Behind the diffuser, an axial-flow compressor was used to regulate the flow. For low flow rates, however, it was necessary to use an orifice behind the compressor to restrict the flow. From the compressor, the air passed through the tail pipe and returned to the wind-tunnel stream.

In order to measure the pressure losses and flow rates at the intake, a rake was placed in the left duct 2.1 inches behind the leading edge of the inlet lip. The rake consisted of 30 total-pressure and 30 static-pressure tubes. A rake at the exit consisted of 33 total-pressure and 8 static-pressure tubes. At each rake, four thermocouples measured the stagnation temperature to verify the assumption of adiabatic flow from free stream to the inlet, and to determine the energy input to the exit air by the compressor.

In this report, data will be shown for the inlets with boundary-layer deflectors on the ramps, the -3° lip angle, and in the forward location only. (See fig. 2.) The lip coordinates (fig. 3) are given for the -3° lip angle.

RESULTS AND DISCUSSION

Data Corrections

The Mach number calibration for the tests was obtained from a survey of the wind tunnel without the model in place and corrected

for constriction effects due to the presence of the model by the methods of reference 4. No other corrections were made to the data for tunnel-wall effects. Because of these effects, the uncorrected angle of attack of the model is approximately 10 percent smaller than it would be in free air for the same lift on the wing.

Model Without Inlets

Extensive pressure measurements were made for the model without inlets to determine the pressure fields in the regions where the submerged inlets were placed. These data will be discussed in relation to all four locations of the submerged inlets and will be referred to in subsequent reports describing the characteristics of the inlets in locations other than shown in the present report. The pressure-distribution data for the wing are located in terms of fuselage station in order to make them directly comparable with the data for the fuselage surface. The data for the wing extend from the leading edge to 95 percent of the wing chord.

The wing pressure distribution (fig. 4) and the tuft pictures (fig. 5) indicate that separation occurred at approximately fuselage station 50 at the low Mach numbers and high angles of attack. At 0.30 Mach number this separation was observed visually to occur at 12-1/2° angle of attack. With increasing Mach number to 0.875, the point of separation moved aft to approximately fuselage station 60 and the angle of attack for separation was reduced to 1°. Separation is indicated on the pressure-distribution plots by the sudden decrease in the adverse pressure gradient. The pressure distribution over the fuselage surface (fig. 6) shows characteristics similar to that over the wing, separation having occurred at approximately the same angle of attack and fuselage station. Because of the poor flow along the fuselage aft of station 50 at the high angles of attack, it is expected that the efficiency of the inlet at the most aft location, fuselage station 59.00, and perhaps of the inlet at fuselage station 50.75, will be poor for such conditions.

The data for the fuselage surface show that up to 6° angle of attack the pressures in the region in which the ramp and inlet for the most forward location were placed (stations 13.15 to 34.25) were almost unaffected by the pressure field of the wing. In addition, forward of station 34.25 the critical pressure coefficient was not exceeded for Mach numbers up to 0.875, the limit of the tests. The data for 0.875 Mach number indicate that the critical Mach number of the fuselage surface forward of station 34.25 was approximately 0.97.

Aft of fuselage station 34.25 the influence of the wing pressure field on the fuselage pressures was strong. At high Mach numbers and large angles of attack, local Mach numbers as high as 1.35 were reached on the fuselage surface and supersonic flow extended for as much as 16 inches along the fuselage surface in which the ramps for the aft locations of the inlets were placed. Therefore, the characteristics of the inlets in the aft location may give an indication of the effect of Mach number on their characteristics in the forward location at free-stream Mach numbers higher than obtained during this investigation.

The measurements of the boundary layer on the fuselage, shown in figure 7, were made separately at the three fuselage stations and simultaneously at the three vertical positions. The data show that, as the Mach number was increased, the boundary-layer thickness increased. This change is attributed to a forward movement of the transition point on the fuselage with increasing Reynolds number. The Reynolds number per foot increased with Mach number from 2.0×10^6 at 0.30 Mach number to 3.9×10^6 at 0.875 Mach number. At the three positions at stations 20.0 and 59.0 and the top position at station 42.5, the boundary layer, in general, also increased with angle of attack, but at the center and bottom positions at station 42.5 the opposite was true. The latter characteristic was probably due to the increase of the favorable pressure gradient with angle of attack at station 42.5.

Inlet at Station 34.25

Ram-recovery ratio.- Due to the large variation of total pressure and mass flow across the entrance of the submerged inlet, the ram-recovery ratio is based upon an effective total pressure at the entrance. The method of computing the effective total pressure is discussed in Appendix A.

Figures 8, 9, and 10 show that the ram-recovery ratio was affected greatly by variations in the mass-flow coefficient[1], but only slightly by Mach number and angle-of-attack variations in the range of the tests. The effect of increasing the mass-flow coefficient was to increase sharply the ram-recovery ratio from approximately 0.50 with zero flow to approximately 0.90 with 0.6 mass-flow coefficient. With greater flows, the ram-recovery ratio

[1]Mass-flow coefficient is defined as the ratio of the mass of air flowing through the duct to the mass of air in the free stream flowing through an area equal to the entrance area of the inlet.

increased slowly, reaching a maximum value with approximately a mass-flow coefficient of 1.0. The highest value of ram-recovery ratio obtained for the forward inlet location was 0.965 at 0.30 Mach number, 0° angle of attack, and 1.0 mass-flow coefficient.

The large reduction in ram recovery for less than 0.6 mass-flow coefficient and the relatively small gain in ram recovery for greater than 0.6 mass-flow coefficient indicates that the most satisfactory design mass-flow coefficient for this installation would be in the region of 0.6. Above about 0.6 mass-flow coefficient, the increase in diffuser losses from the inlet to the compressor face would probably offset the reduction in entry losses; whereas, below 0.6 mass-flow coefficient, the opposite would be true.

It is believed that for the mass-flow coefficients near zero, the true ram-recovery ratios were higher than the measured values. This belief is substantiated by the fact that with these low flow rates the static pressure in the diffuser was somewhat higher than the measured total pressure at the entrance, the difference being of the order of 10 percent of free-stream ram pressure. The discrepancy at the low flow rates is believed to be due either to a rapid fluctuation of the flow at the entrance, which was not measured and which would be damped out at the compressor, or to an angularity of the flow at the entrance with respect to the total-pressure tubes.

An instability of flow through the twin-inlet installation used on this model was observed for flow coefficients less than 0.4. With the tail rake substantially indicating a constant total rate of flow through both inlets, the rake at the left inlet indicated changes in the flow rate from zero to that equal to the rate at the exit as the angle of attack was changed. Flow instability in an airplane installation is undesirable, since a pressure or velocity variation around the face of the compressor may damage the compressor. Snaking of the airplane or increases in the induction-system losses also may be caused by the instability. The cause of flow instability and means of eliminating it are discussed in reference 5.

Figure 9 shows the small effect that variations in angle of attack had on the ram-recovery ratio. In all but a few cases the ram-recovery ratio changed less than 0.03 with variation in angle of attack. With a constant mass flow, the maximum recovery was obtained in the region of 0° angle of attack. This characteristic is accounted for by the fact that in this angle-of-attack range the boundary layer

on the fuselage sides ahead of the inlets was the smallest. Another reason will be shown when discussing the pressure distribution along the ramp.

The effect of Mach number on the ram-recovery ratio (fig. 10) was small up to the limits of the test, 0.875 Mach number. There was a small decrease in the recovery ratio with increasing Mach number from 0.30, but this decrease usually amounted to less than 0.03 throughout the Mach number range. This small decrease can be attributed to the increase in boundary-layer thickness along the fuselage surface in the region of the inlet as the Reynolds number increased with Mach number.

Entrance ram-recovery contours and ramp pressure distribution.- The contours in figure 11 are presented to show the distribution of pressure loss and flow at the entrance of one of the submerged inlets for typical test data. The data were arranged so that, in each group of three parts of figure 11, one parameter was variable and the other two parameters were approximately constant. In order to simplify the drawings, the entrance is shown as a rectangle, although on the actual installation the upper and lower sides of the entrances were straight and parallel and the ramp side and lip side were curved.

It will be noticed in several of the contour plots (e.g., figs. 11(b) to 11(e)) that there are regions about one quarter of the duct width from both the upper and lower sides of the duct in which the losses seem more pronounced. These regions have been more positively identified in low-speed tests of a larger submerged inlet in which it was possible to take more pressure measurements. The regions are believed to be caused by the air along the fuselage surface spilling over the edges of the ramp and mixing with the air passing along the ramp. The deflectors used on the ramp for the installation discussed in this report should tend to minimize this effect.

In each group of three contour plots in figures 11(a),(b),(c) to figures 11(p),(q),(r), Mach number is the variable parameter. Although within each group the mass-flow coefficients are not identical, it is believed that within the groups containing the higher mass-flow coefficients they are sufficiently close together to show the effects of Mach number on ram recovery, since in this region the ram-recovery ratio varied little with mass-flow coefficient. For the low mass-flow coefficients, however, small changes in the flow rate obscure the effect of Mach number. Therefore, conclusions made with respect to the effect of Mach number are not verified in the groups containing the lowest mass-flow coefficients because of the variation in mass-flow coefficient. The data show that with increasing Mach number,

the pressure losses increased in the upper and lower inside corners. (E.g., see figs. 11(d), (e), and (f).) This characteristic is believed to be due to the boundary layer along the ramp, which probably increased in thickness with Reynolds number similarly to that indicated along the fuselage surface (fig. 7), being pushed into the corners by the higher pressure along the center of the ramp (fig. 12). The increase of losses in the corner may also be due to the fact that the critical Mach numbers of the upper and lower walls of the ramp were lower than that of the ramp. Just above the critical Mach numbers, shocks may occur on both walls of the ramp but not at the center of the ramp, thereby increasing the losses in the corners. It should be mentioned, however, that the critical pressure coefficient was computed, assuming that the free-stream total pressure existed at the point at which the static pressure was measured, since total pressures were not measured along the ramp but only at the entrance. Any total-pressure losses in the air as it passed along the ramp would make the critical pressure coefficient more negative and therefore increase the critical Mach number above that indicated in figure 12. For this reason, it is believed that the main cause for the increasing losses in the corners as the Mach number increased was the thickening of the boundary layer.

The data of figures 11(a), (b), and (c) show that for the low rates of flow and negative angles of attack, most of the pressure losses were in the lower inside corner of the entrance; whereas at 2° angle of attack (figs. 11(s) and (t)), the losses were in the upper inside corner. The losses in these corners were due to separation of the flow from the walls of the ramp. In figures 12(d) and (h), the sudden decrease in the adverse pressure gradient in the region of station 30 on the lower wall indicates separation for −2° angle of attack and 0.80 and 0.875 Mach number. Similar characteristics were noted for −2° angle of attack at other Mach numbers during the investigation. Separation from the upper wall of the ramp for 2° angle of attack is also indicated in figures 12(c) and (e). However, at angles of attack greater than 2°, no separation from either the upper or lower walls of the ramp was evident. This characteristic is shown for 0.80 Mach number (fig. 12(f)) and was also noted at other Mach numbers. In addition, no separation is indicated at 0° angle of attack. It was the separation from the upper and lower walls of the ramp occurring only at negative angles and around 2° angle of attack which probably accounted for the ram-recovery ratio being lower there than in the remainder of the test angle-of-attack range. (See fig. 9.)

Pressure distribution on fuselage surface and lip.- In figure 13 the pressure distributions along the fuselage surface and on the lip of the inlet are shown. It will be noticed that the pressure

coefficients in front of the lip at water lines 3.2 and −3.2 were less negative than those along the ramp center line (Water Line 0, fig. 12) at the same Mach number and angle of attack. Therefore, the critical pressure coefficient would be exceeded first at the ramp center line. However, all of the air entering the inlet did not pass along the ramp, for some of it passed along the fuselage surface and spilled over the ramp edges into the inlet. It is believed, therefore, that even after the critical pressure coefficient has been exceeded somewhat on the ramp center line and a shock wave has formed, the ram-recovery ratio at the inlet will not be decreased seriously because all the entering air will not have passed through the shock. Since the critical Mach number of the ramp was approximately 0.875 and that at water lines 3.2 and −3.2 adjacent to ramp was approximately 0.94, the ram-recovery characteristics of the submerged inlets in the forward location should continue to be good at Mach numbers somewhat above the maximum of these tests.

Maintaining good recovery at Mach numbers above those of the tests presupposes that the critical Mach number of the inner surface of the lip has not been exceeded. A shock forming on the inner surface of the lip would cause large losses at the inlet and probably reduce the efficiency of the diffuser. Pressure-distribution data for the inner surface of the lip (fig. 13) indicate that the critical Mach number depended on the mass-flow coefficient, as well as the free-stream Mach number, but was almost independent of angle of attack. With a mass-flow coefficient of 1.04, the critical Mach number was 0.70. Decreasing the mass-flow coefficient to 0.91 increased the critical Mach number almost linearly to 0.875. These values of mass-flow coefficient at the critical Mach number are slightly higher than it was possible to obtain when the rake was in the entrance. The effect, therefore, on ram-recovery ratio at the inlet of exceeding the critical Mach number of the inner surface of the lip is not known. The lack of data in this region is not serious, however, since the mass-flow coefficients at the critical Mach number of the lip were above those which would occur in flight.

A comparison of figures 6 and 13 indicates that the pressure coefficients at water lines 3.2 and −3.2 forward of station 34.25 were made more negative by the presence of the ramp, thus lowering the critical Mach number of the fuselage in this region. Without the ramp in place, the critical Mach number was approximately 0.97; whereas with the ramp in place, it was approximately 0.94.

Increment of drag coefficient. – In figure 14, the increment of drag coefficient based on wing area due to the submerged inlets with deflectors is shown. The drag increments were computed by

subtracting the drag of the model without the inlets, and with a tail cone at the exit from the external drag of the model with the inlets in place, the tail cone removed, and air flowing through the model. Since there was no way to separate the drag of the inlets from the drag of the exit, the drag increments presented show the external effect of placing the complete air-induction and exhaust system in the streamlined body. The drag of the aft portion of the fuselage may have varied with the mass-flow coefficient because of changes in the static pressure at the exit or the external flow in the vicinity of the exit. This effect should be small, however, as the change in exit velocity was small because the exit area was 2.45 times as large as the entrance area. The method of computing the external drag of the model is discussed in Appendix B.

The data indicate that the increment of drag coefficient decreased with increasing mass-flow coefficient and, generally speaking, was approximately 0.005 at 0.2 mass-flow coefficient and 0.001 at 1.0 mass-flow coefficient. Reference 3 shows that this increment of drag coefficient could be reduced by improving the shape of the deflectors. The effect of mass-flow coefficient was about the same up to a Mach number of 0.825. At 0.825 Mach number and above, the increment of drag coefficient increased over part of the mass-flow range. This apparent change in the drag characteristics at high Mach numbers may be due to experimental errors as the drags of the model with or without the inlets are large and unsteady at high Mach numbers, and small percentage errors in the measurements may have caused large errors in their difference.

CONCLUSIONS

A wind-tunnel investigation up to 0.875 Mach number of NACA submerged inlets on a fuselage with the entrances 16.7 percent of the root chord ahead of the wing-root leading edge indicated the following:

1. The ram-recovery ratio at the entrance was affected greatly by variation in the mass-flow coefficient. Representative values of the ram-recovery ratio were 0.50 at zero flow, 0.90 at 0.6 mass-flow coefficient, and 0.95 at 1.0 mass-flow coefficient.

2. Variations of Mach number and angle of attack, in general, caused less than a 0.03 variation in the ram-recovery ratio.

3. The increment of drag coefficient, due to the submerged inlets with deflectors, decreased with increase in mass-flow

coefficient. Representative values of the increment were 0.005 at 0.2 mass-flow coefficient and 0.001 at 1.0 mass-flow coefficient.

Ames Aeronautical Laboratory,
National Advisory Committee for Aeronautics,
Moffett Field, Calif.

APPENDIX A

Effective Total Pressure at Inlet

The total pressure was not constant across the inlet area because some of the air, in flowing along the fuselage in front of the inlet, had lost some of its pressure energy and thereby increased its entropy. It was therefore necessary to calculate an effective total pressure which represented the same energy loss and entropy gain for the entire stream entering the inlet as was obtained by summing the values of these parameters for the various stream tubes.

The total energy and the entropy gain in the stream are given by the following equations:

$$E_1 = \frac{\gamma}{\gamma-1} \int \frac{H'_1}{\rho_s} \, dm \tag{A1}$$

$$\Delta s_1 = \int c_p \log_e \left[\left(\frac{T'_1}{T_o} \right) \left(\frac{H_o}{H'_1} \right)^{2/7} \right] dm \tag{A2}$$

Since it was not possible to determine ρ_s independent of H'_1, the energy equation was eliminated as a means of finding H_1, the effective total pressure.

It was found from temperature measurements at the inlet that $T'_1 = T_o$. Equation (A2) was then simplified as follows:

$$\Delta s_1 = \int \frac{2}{7} c_p \log_e \left(\frac{H_o}{H'_1} \right) dm \tag{A3}$$

Since the effective total pressure represents the same entropy gain,

$$\frac{2}{7} c_p \log_e \left(\frac{H_o}{H_1}\right) \int dm = \int \frac{2}{7} c_p \log_e \left(\frac{H_o}{H'_1}\right) dm \qquad (A4)$$

The above equation was simplified by removing the constant quantities from inside the integral and canceling similar quantities on opposite sides of the equation. The resulting equation which was used to determine the effective total pressure is as follows:

$$\log_e H_1 = \frac{\int \log_e H'_1 \, dm}{\int dm} \qquad (A5)$$

In the actual computations, the following assumptions were made:

$$\int \log_e H'_1 \, dm = \sum_{n=1}^{n=30} \log_e H'_n \, \rho_n \, V_n \, \Delta A_n$$

$$\int dm = \sum_{n=1}^{n=30} \rho_n \, V_n \, \Delta A_n$$

since the number of equal areas in which the total pressure was measured was 30.

APPENDIX B

External Drag

The external drag of the model, with air entering the inlets, was calculated by subtracting the internal drag of the ducting system from the drag of the entire model. The internal drag was determined from the equation $D_i = m(V_o - V_4)$ where V_4 is a mean hypothetical velocity of the ducted air when its static pressure has returned to free-stream static pressure with no further loss in total pressure from the exit. The free-stream velocity V_o was used in the above equation in order to make this method for computing the external drag comparable with that used for nose inlets. Therefore, when using performance data for jet engines in conjunction with the external drag for a submerged inlet, the entire ram drag mV_o must be subtracted from the gross thrust to determine the net thrust.

The drag data are presented as increments of drag coefficient due to the inlets. The increments were calculated from the differences between the external drags of the model with the inlets and the drag of the model without inlets but with a tail cone at the exit.

REFERENCES

1. Frick, Charles W., Davis, Wallace F., Randall, Lauros M., and Mossman, Emmet A.: An Experimental Investigation of NACA Submerged-Duct Entrances. NACA ACR No. 5I20, 1945.

2. Mossman, Emmet A., and Randall, Lauros M.: An Experimental Investigation of the Design Variables for NACA Submerged Duct Entrances. NACA RM No. A7I30, 1947.

3. Delany, Noel K.: An Investigation of Submerged Air Inlets on a 1/4-Scale Model of a Typical Fighter-Type Airplane. NACA RM No. A8A20, 1948.

4. Herriot, John G.: Blockage Corrections for Three-Dimensional-Flow Closed-Throat Wind Tunnels, with Consideration of the Effect of Compressibility. NACA RM No. A7B28, 1947.

5. Mossman, Emmet A., and Gault, Donald E.: Development of NACA Submerged Inlets and a Comparison with Wing Leading-Edge Inlets for a 1/4-Scale Model of a Fighter Airplane. NACA RM No. A7A31, 1947.

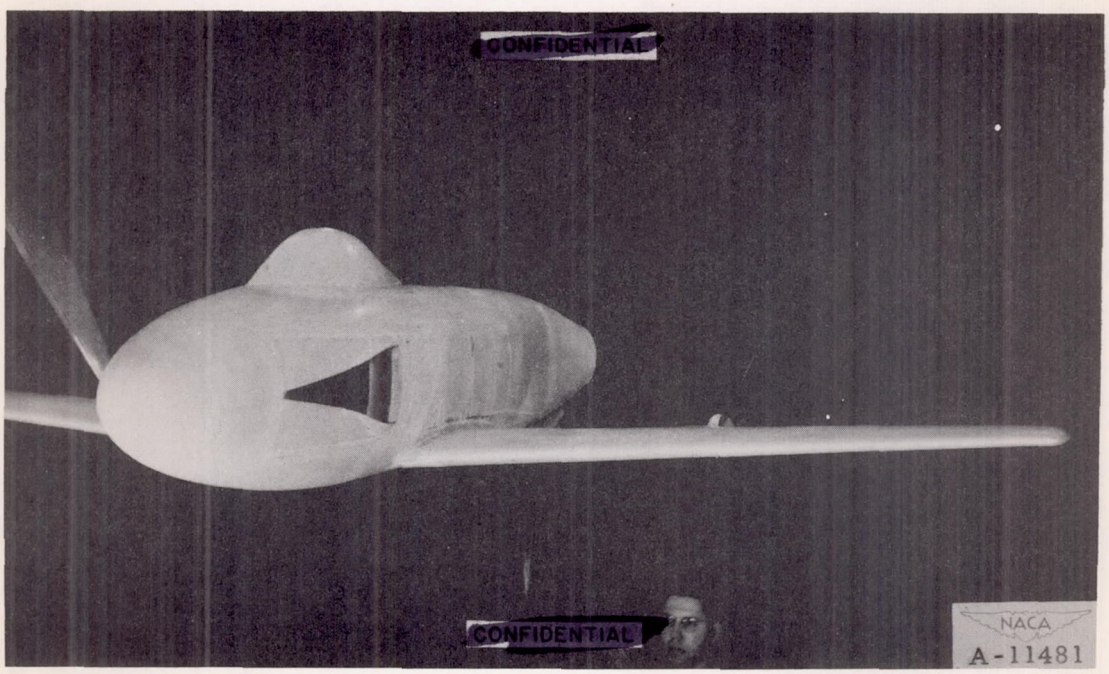

Figure 1.– Model with the inlets at fuselage station 34.25.

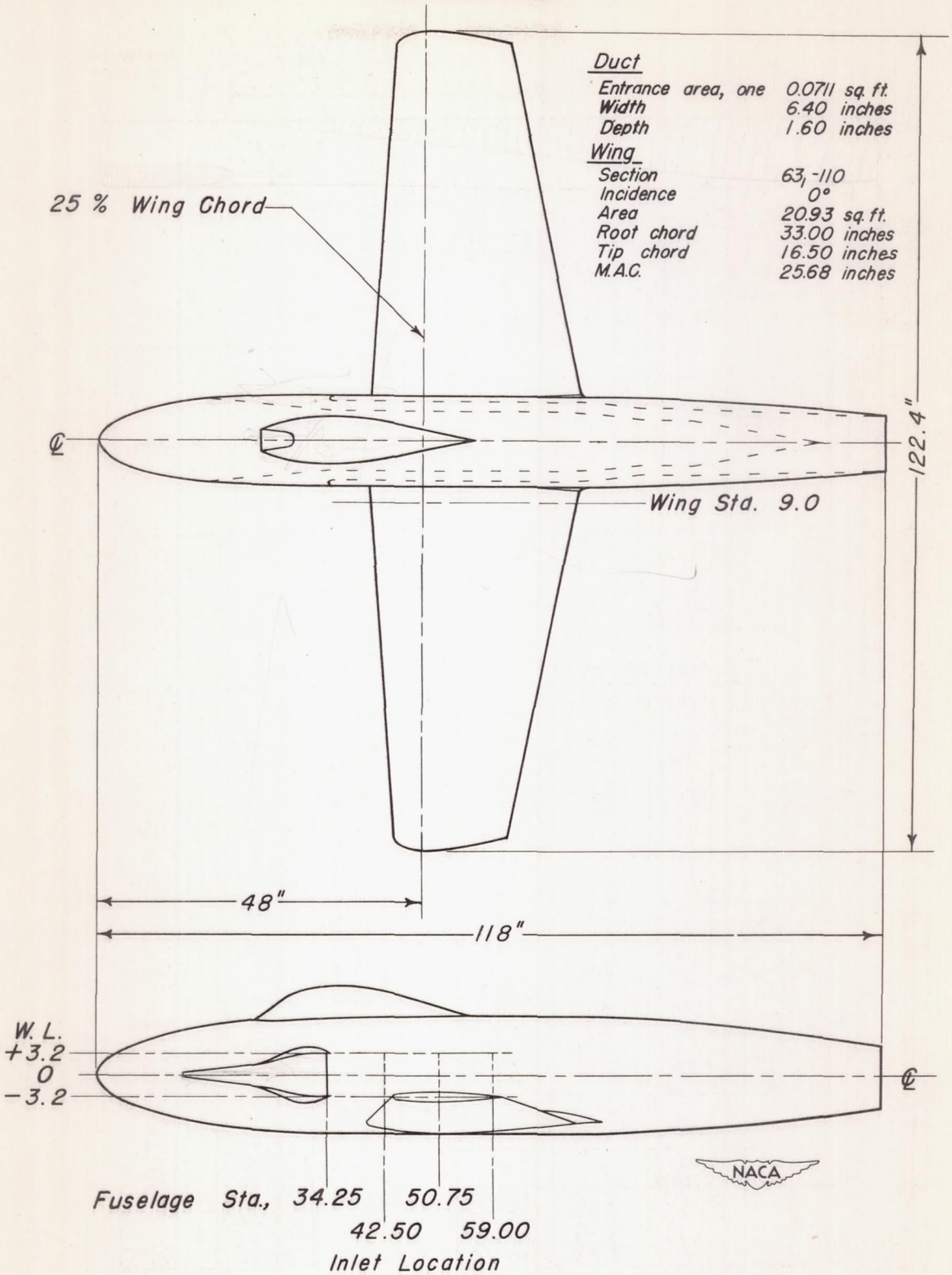

Figure 2.— Submerged-inlet model.

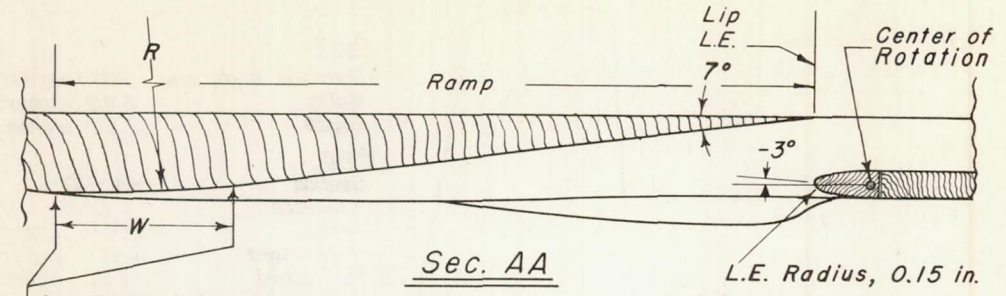

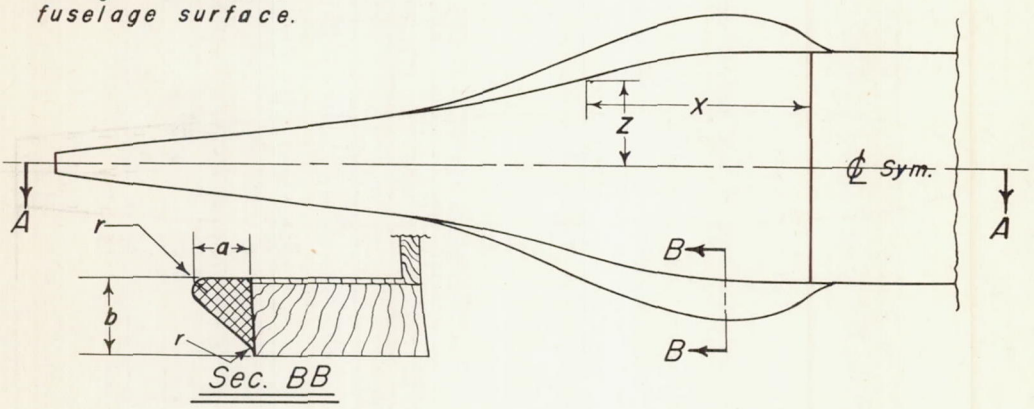

Deflector Coordinates

X-Inches	a-Inches	b-Inches	r-Inches
-.63	0	0	0
-.32	.069	.099	.014
0	.224	.323	.047
.63	.446	.642	.094
1.27	.630	.907	.132
1.90	.721	1.038	.151
2.53	.745	1.073	.156
3.17	.741	1.067	.156
3.80	.723	1.041	.152
4.43	.694	.999	.146
5.06	.648	.933	.136
5.70	.588	.847	.123
6.33	.522	.752	.110
6.96	.452	.651	.095
7.60	.370	.533	.078
8.23	.284	.409	.060
8.86	.200	.288	.042
9.50	.122	.176	.026
10.13	.058	.084	.012
10.76	0	0	0

Lip Coordinates

Station	Outer Surface	Inner Surface
Inches From Nose	Inches From Fuselage Surface	Inches From Fuselage Surface
0	0.372	0.372
0.2	0.193	0.568
0.4	0.131	0.638
0.6	0.085	0.691
0.8	0.055	0.725
1.0	0.032	0.747
1.2	0.015	0.759
1.4	0.004	0.761
1.6	0	0.762
1.8	0	0.762

Ramp Wall Coordinates

X-Inches	Z-Inches
0	3.20
2.11	3.18
4.22	2.93
6.33	2.45
8.44	1.94
10.55	1.55
12.66	1.25
14.77	.99
16.88	.75
18.99	.51
21.10	.27

Ramp Coordinates

No.	Inlet Location	W	R
1	34.25	8.60	32.40
2	42.50	5.02	29.70
3	50.75	3.75	28.85
4	59.00	3.75	30.70

NACA

Figure 3.— Dimensional data for inlets.

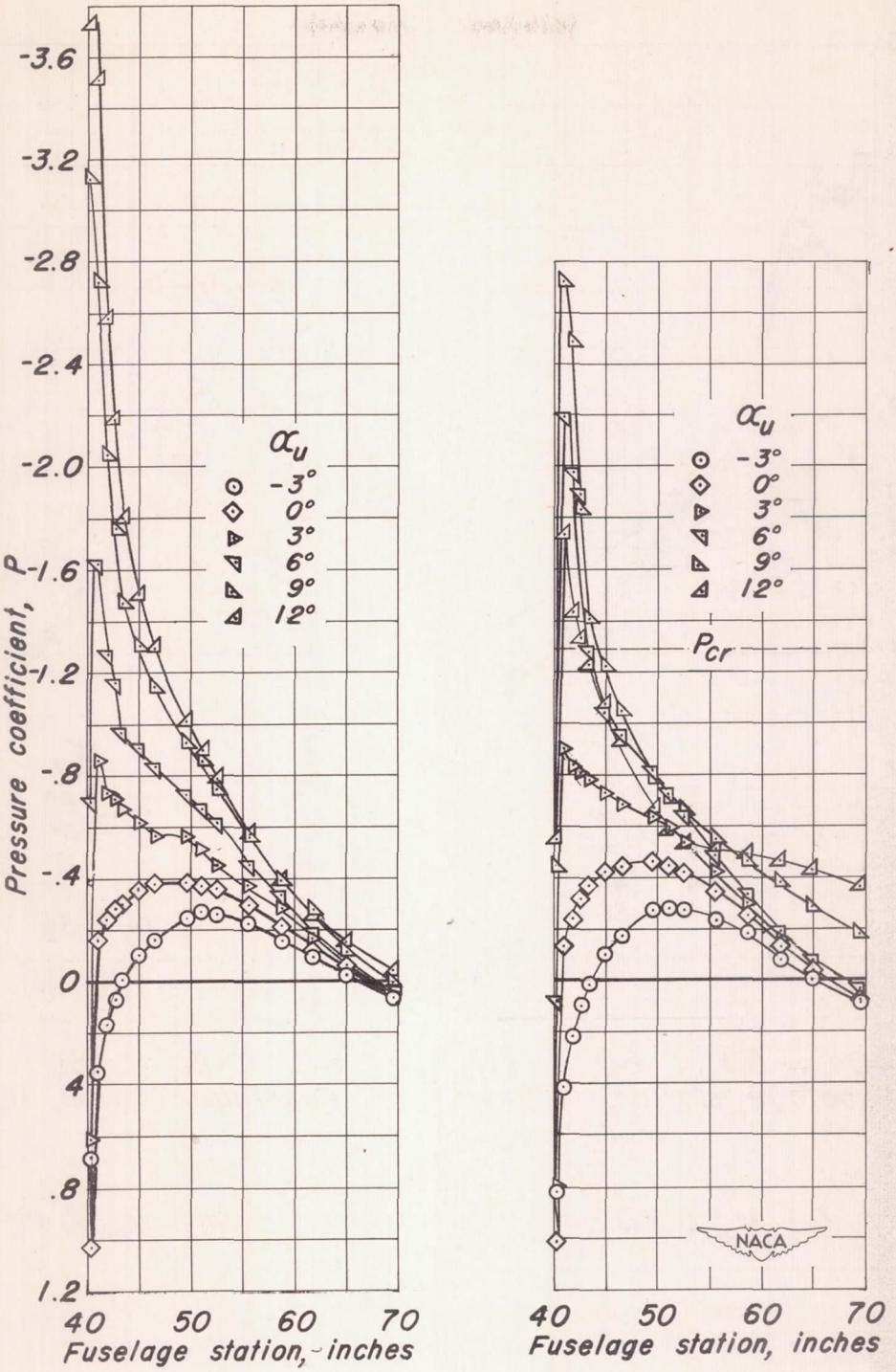

(a) M_0, 0.30 (b) M_0, 0.60

Figure 4.– Pressure distribution on upper surface of wing at station 9.0 with inlets and exit sealed.

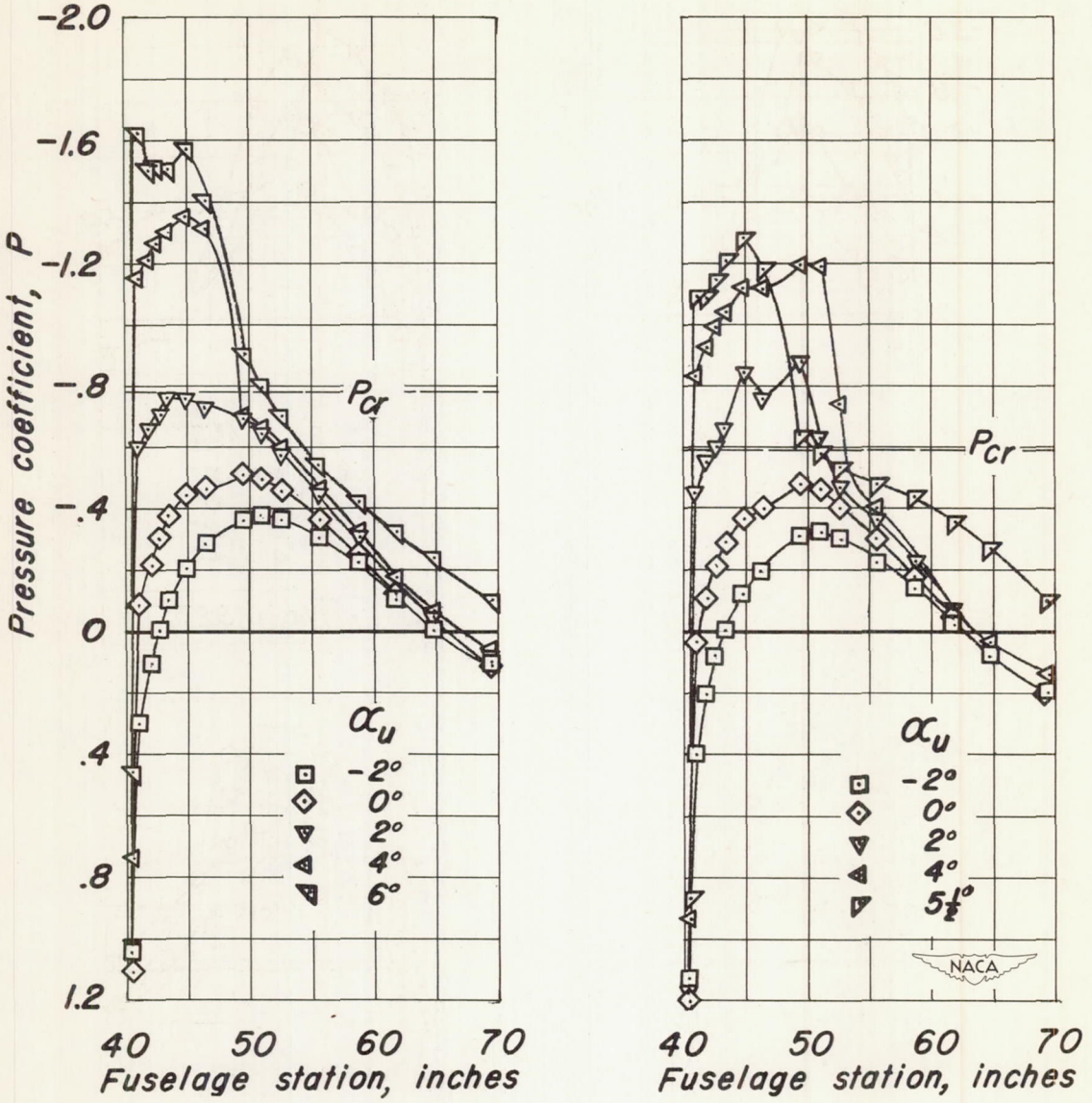

(c) M_0, 0.70

(d) M_0, 0.75

Figure 4. – Continued.

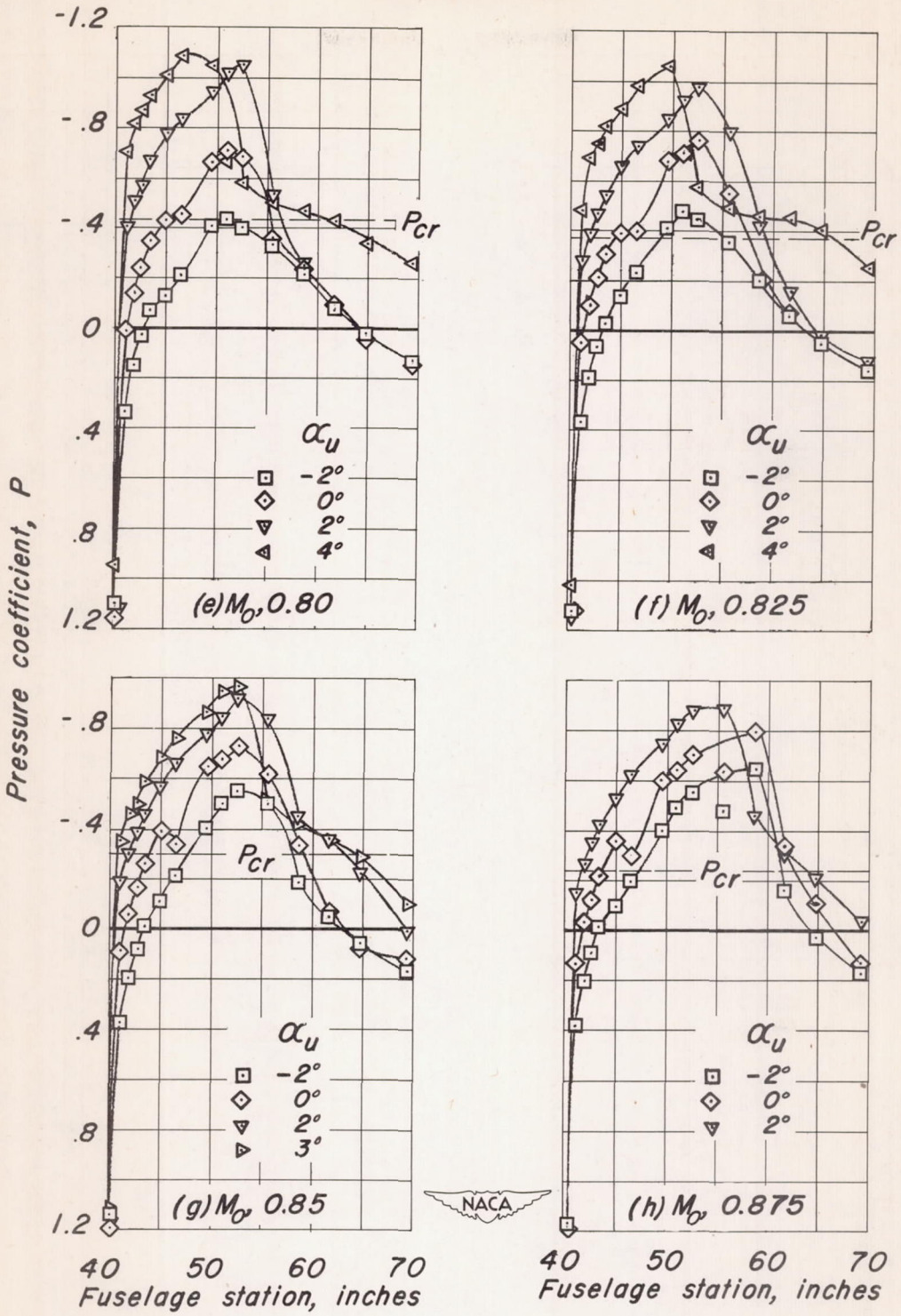

Figure 4. – Concluded.

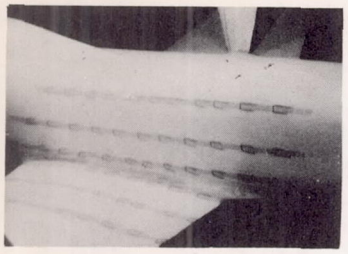

α, 0°

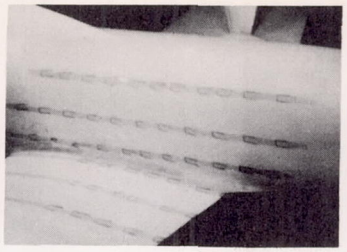

α, 0°

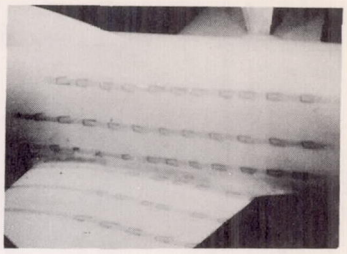

α, 0°

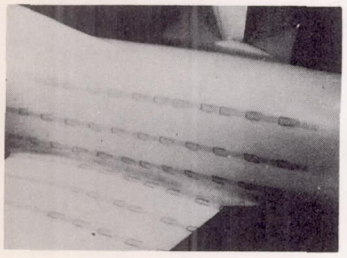

α, 6°

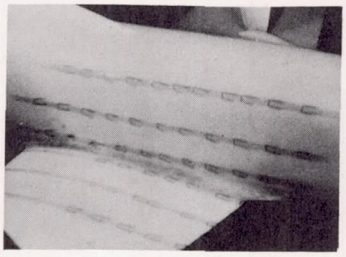

α, 4°

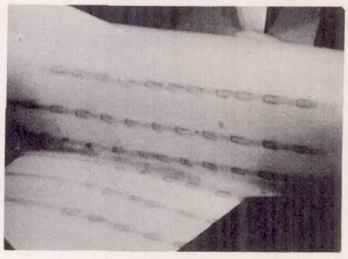

α, 2°

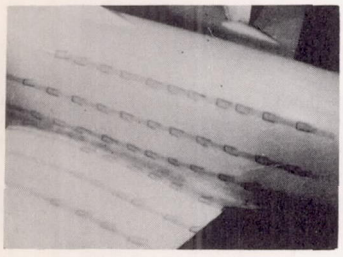

α, 12°

M, 0.30

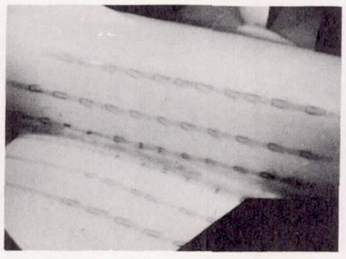

α, 6°

M, 0.70

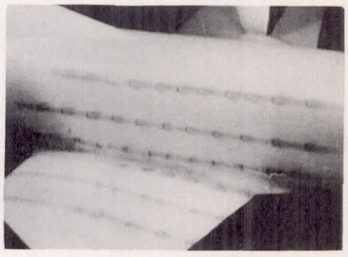

α, 4°

M, 0.80

Figure 5.- Flow over the smooth fuselage.

NACA A-12421

CONFIDENTIAL

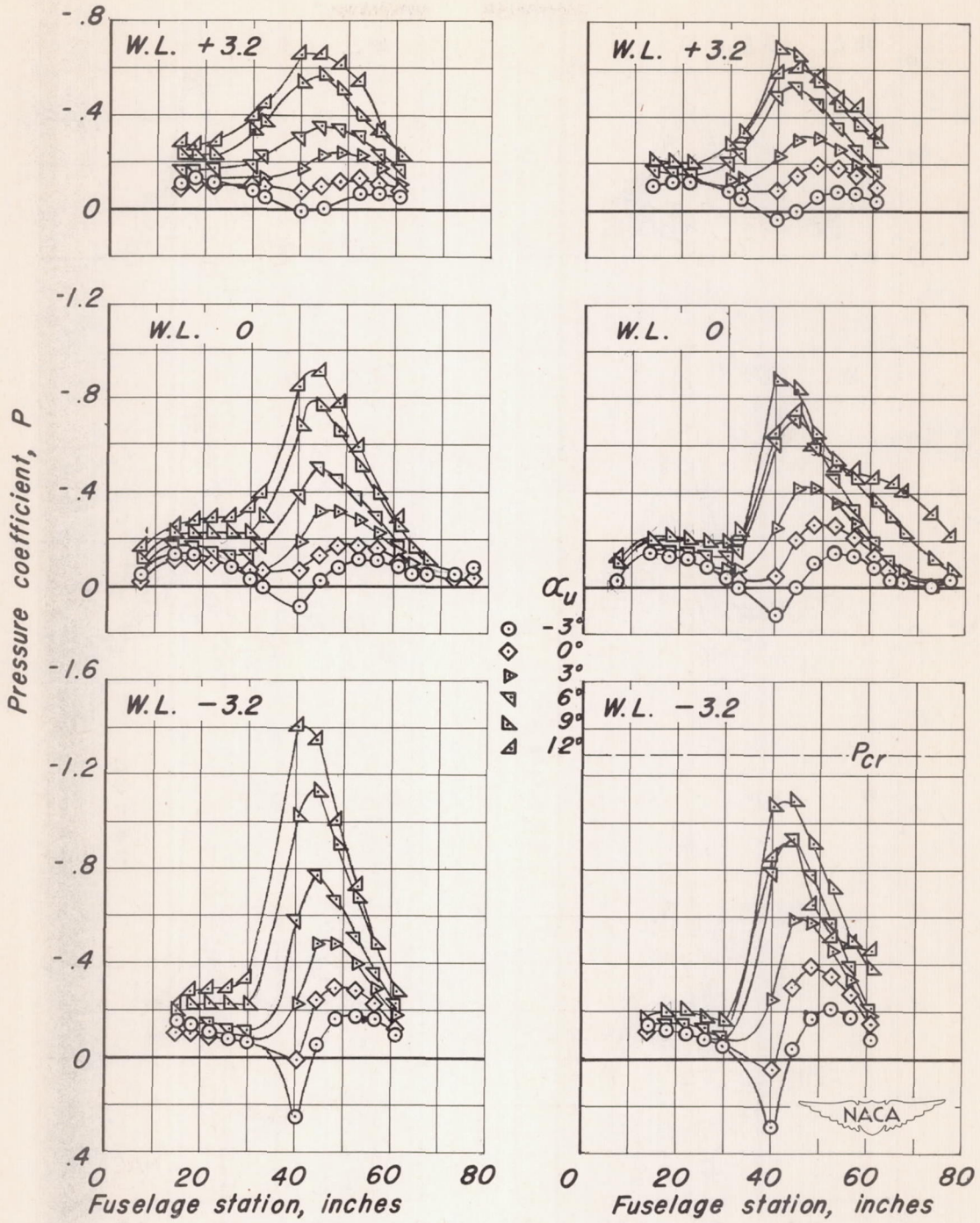

(a) M_0, 0.30 (b) M_0, 0.60

Figure 6.—Pressure distribution along fuselage with inlets and exit sealed

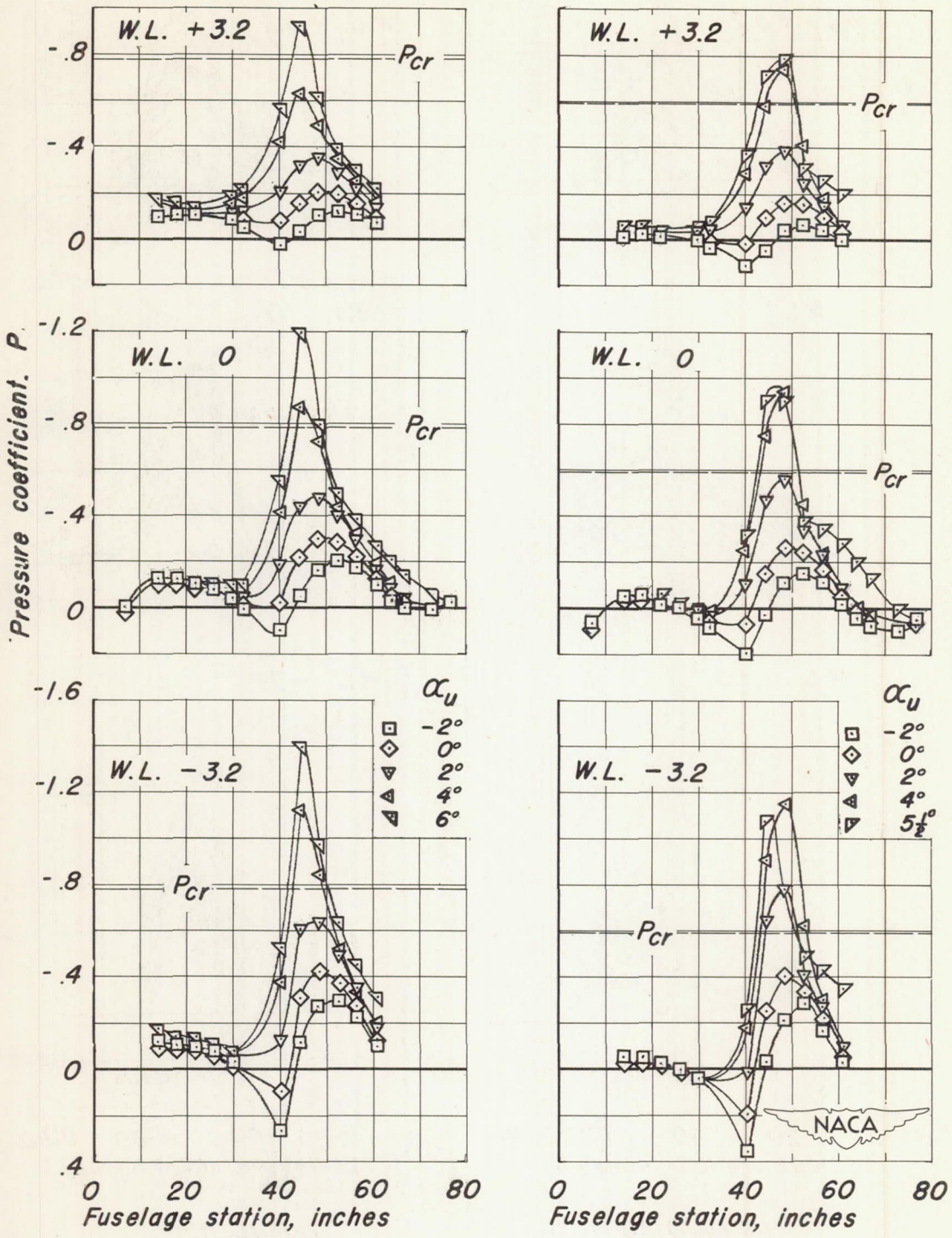

(c) M_o, 0.70

(d) M_o, 0.75

Figure 6. – Continued.

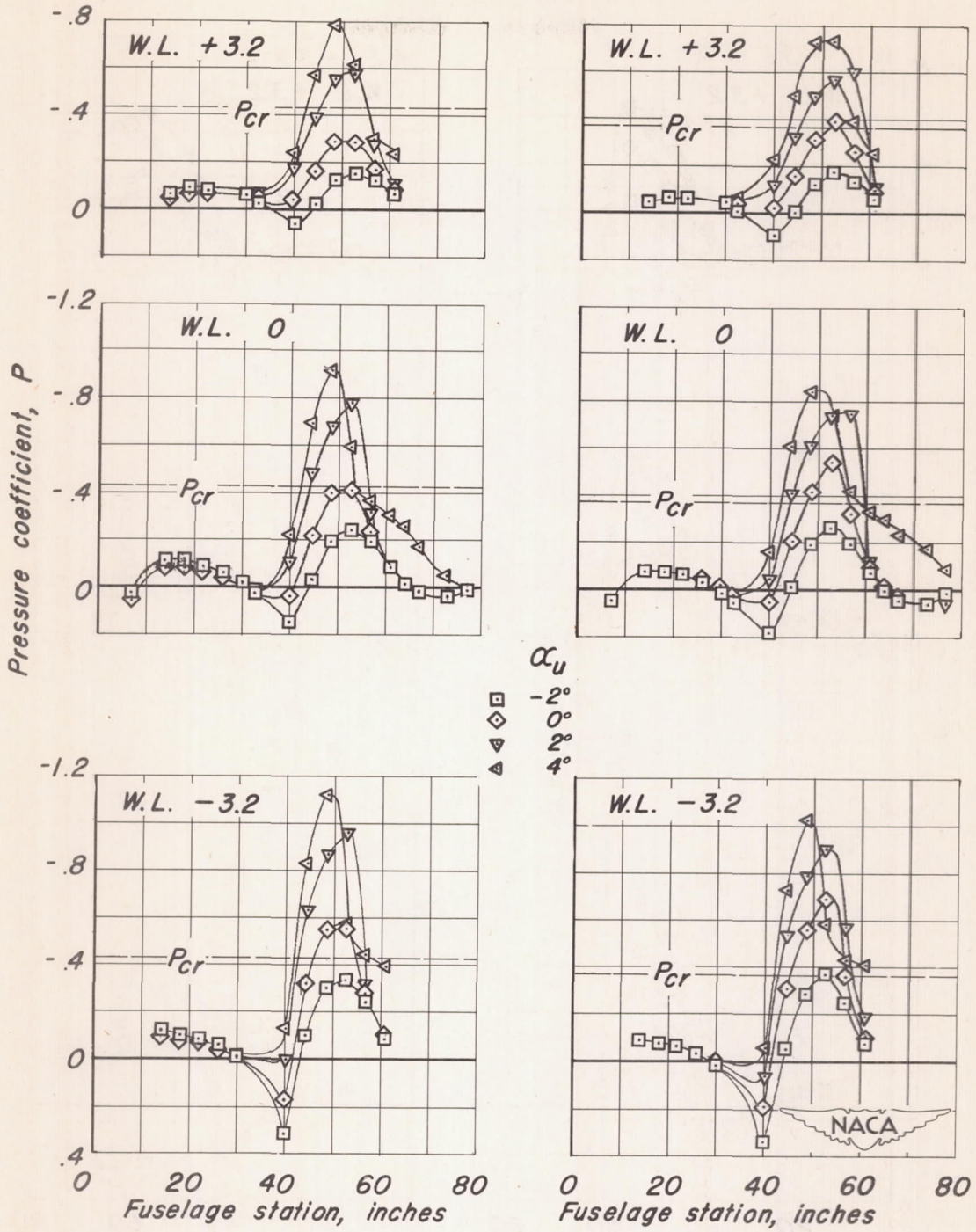

(e) M_0, 0.80 (f) M_0, 0.825

Figure 6. – Continued.

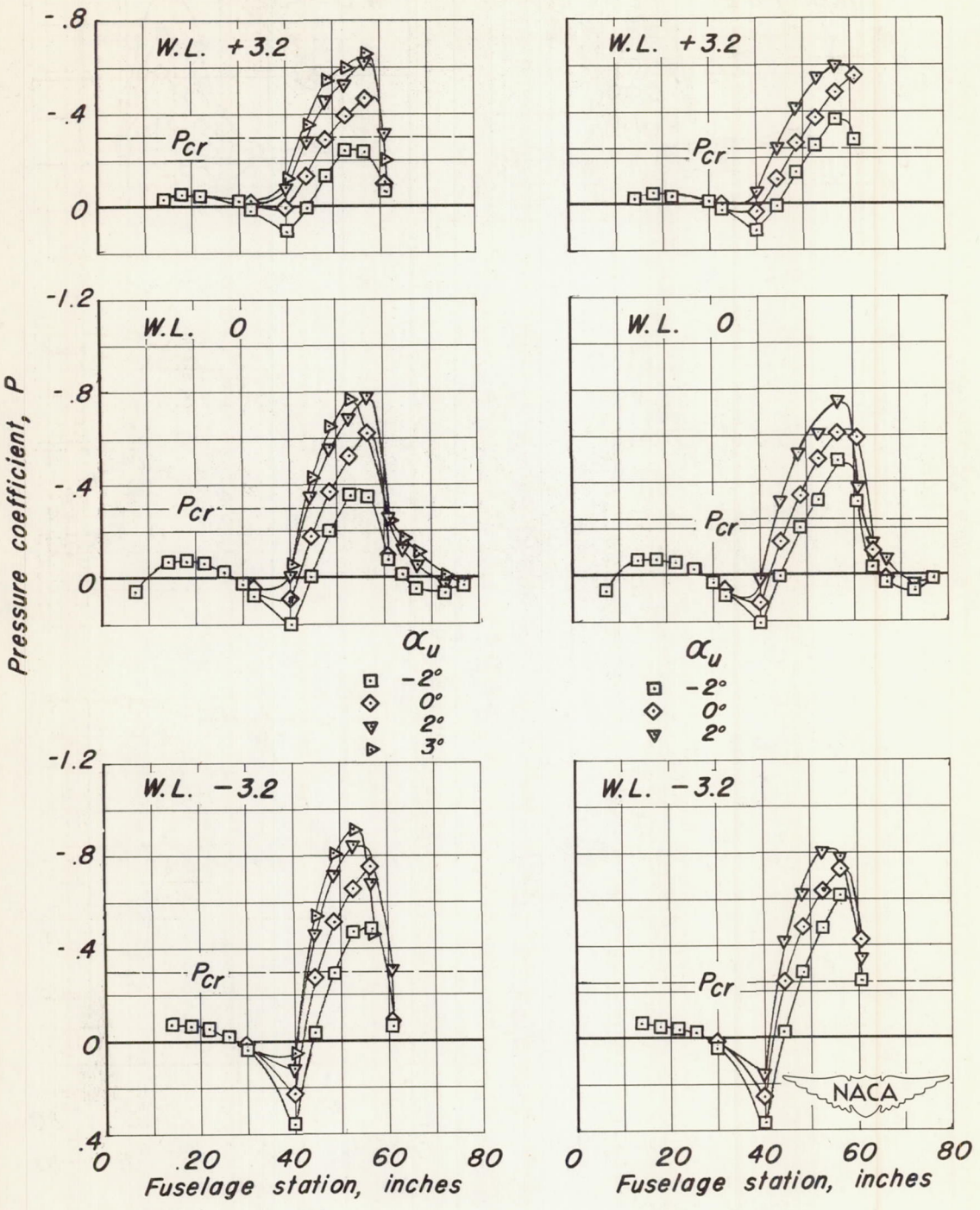

(g) M_0, 0.85 (h) M_0, 0.875

Figure 6. – Concluded.

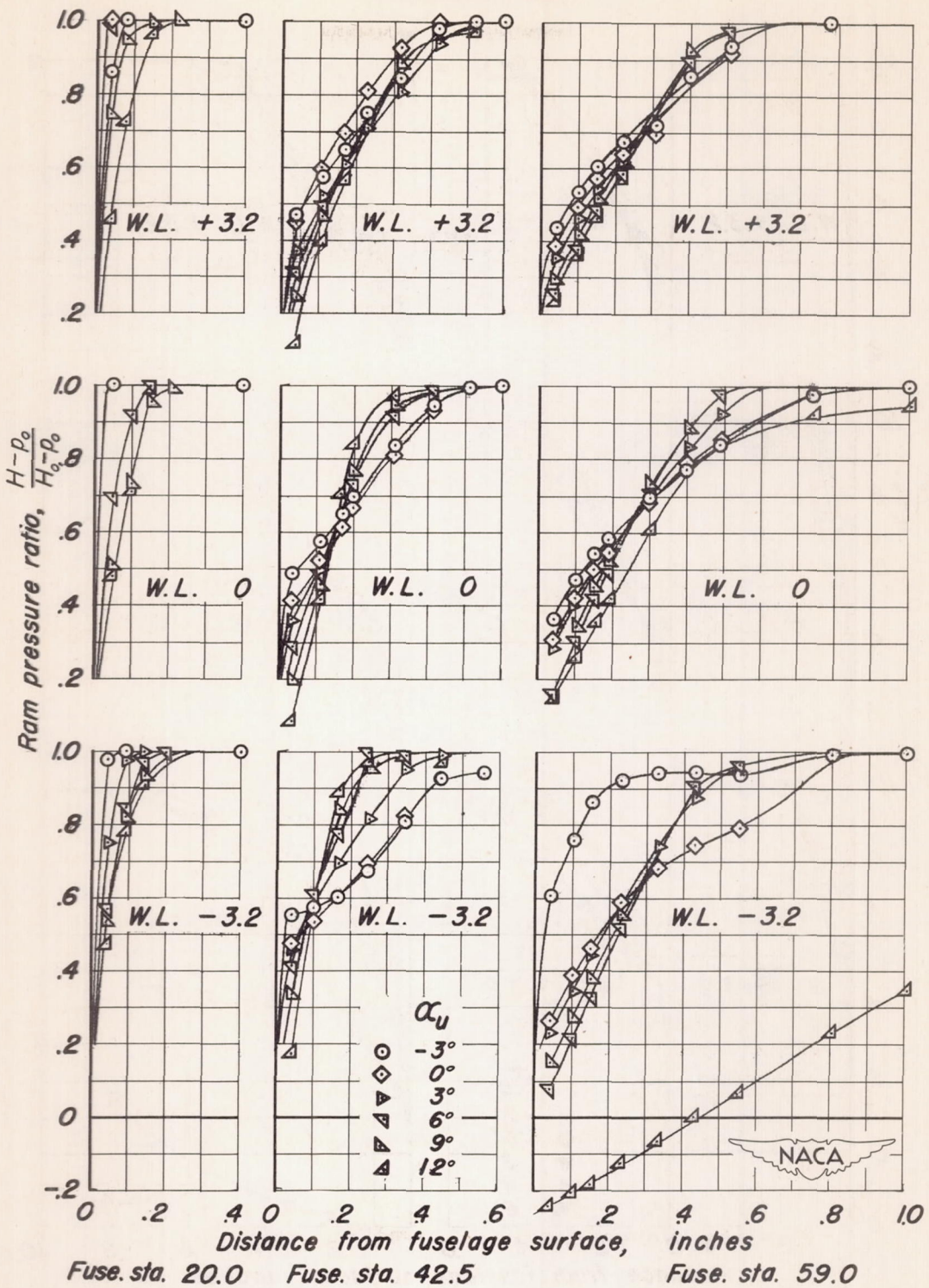

(a) M_0,0.30

Figure 7.– Ram–pressure ratio in the boundary layer along the fuselage with the inlets and exit sealed.

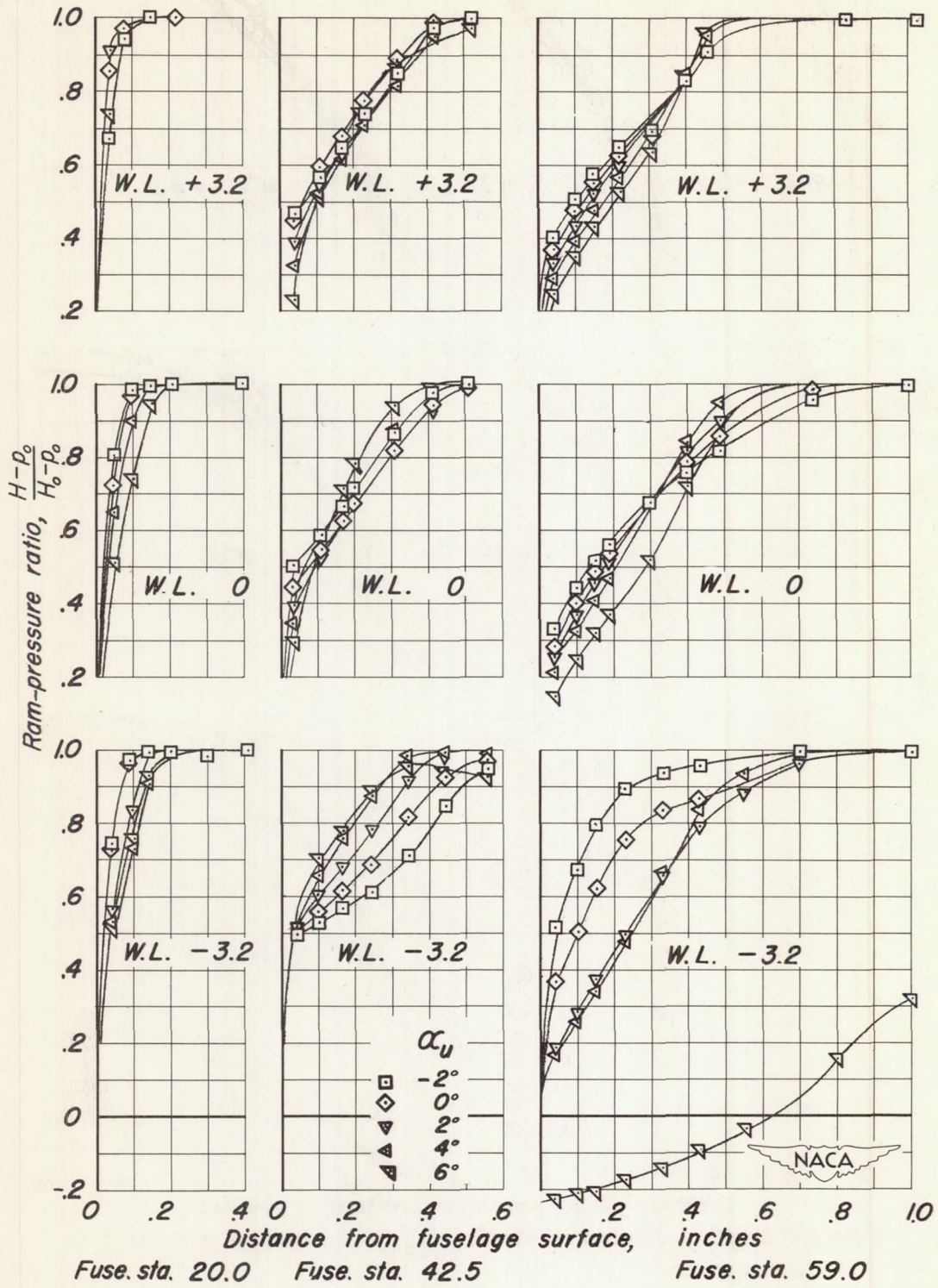

(b) M_o, 0.70

Figure 7. – Continued.

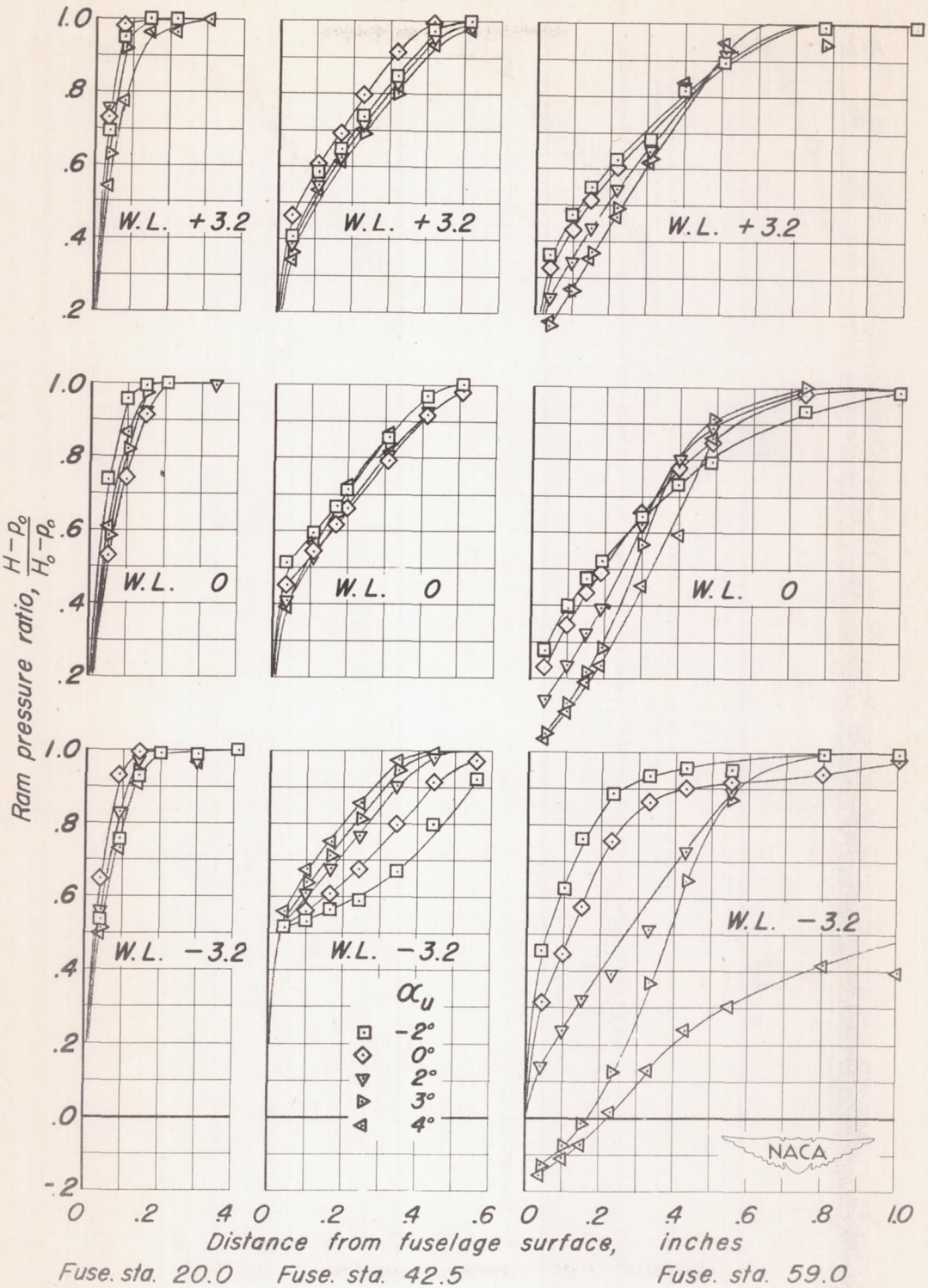

(c) M_o, 0.80

Figure 7. - Continued.

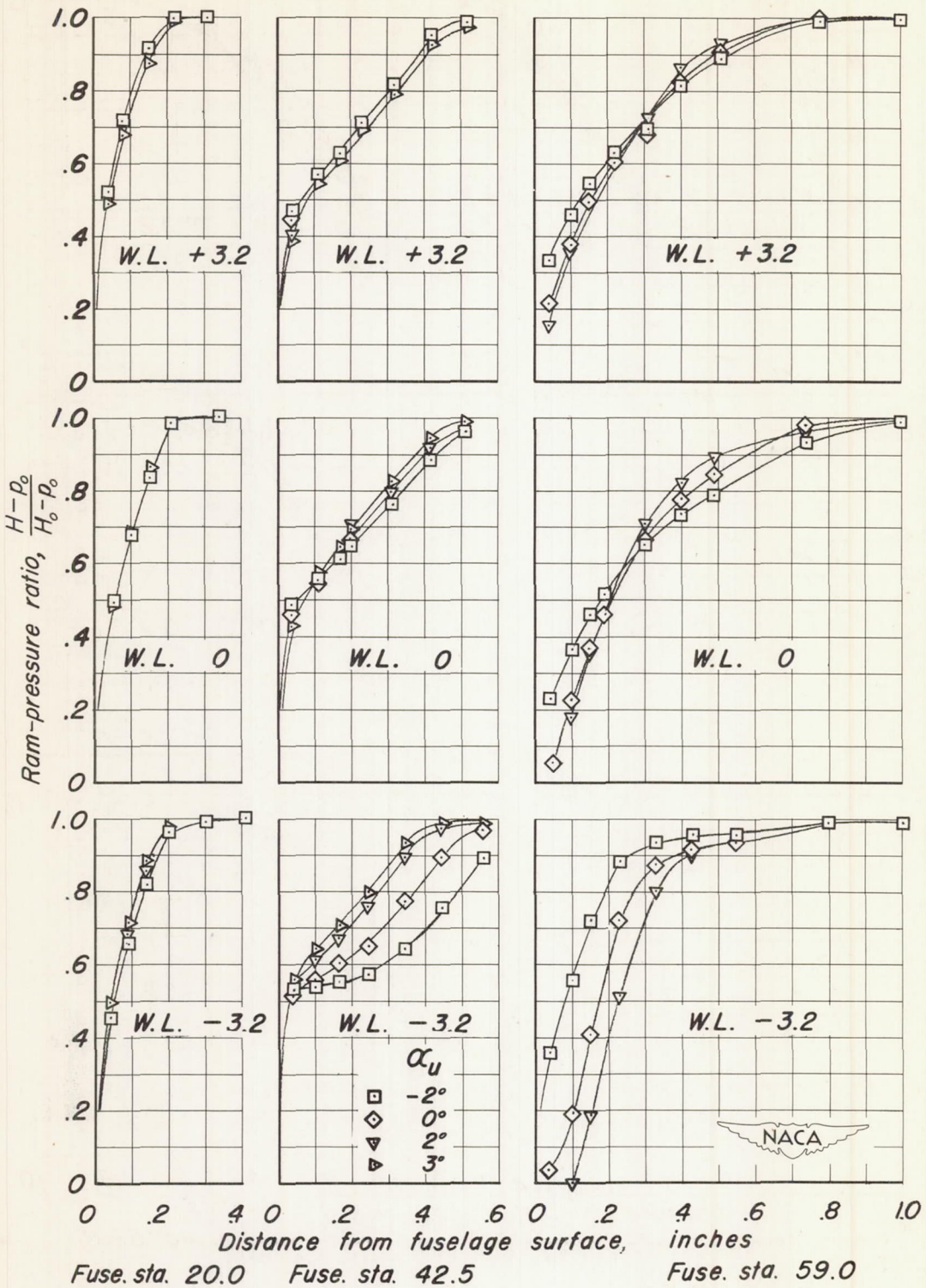

(d) M_o, 0.85

Figure 7. – Continued.

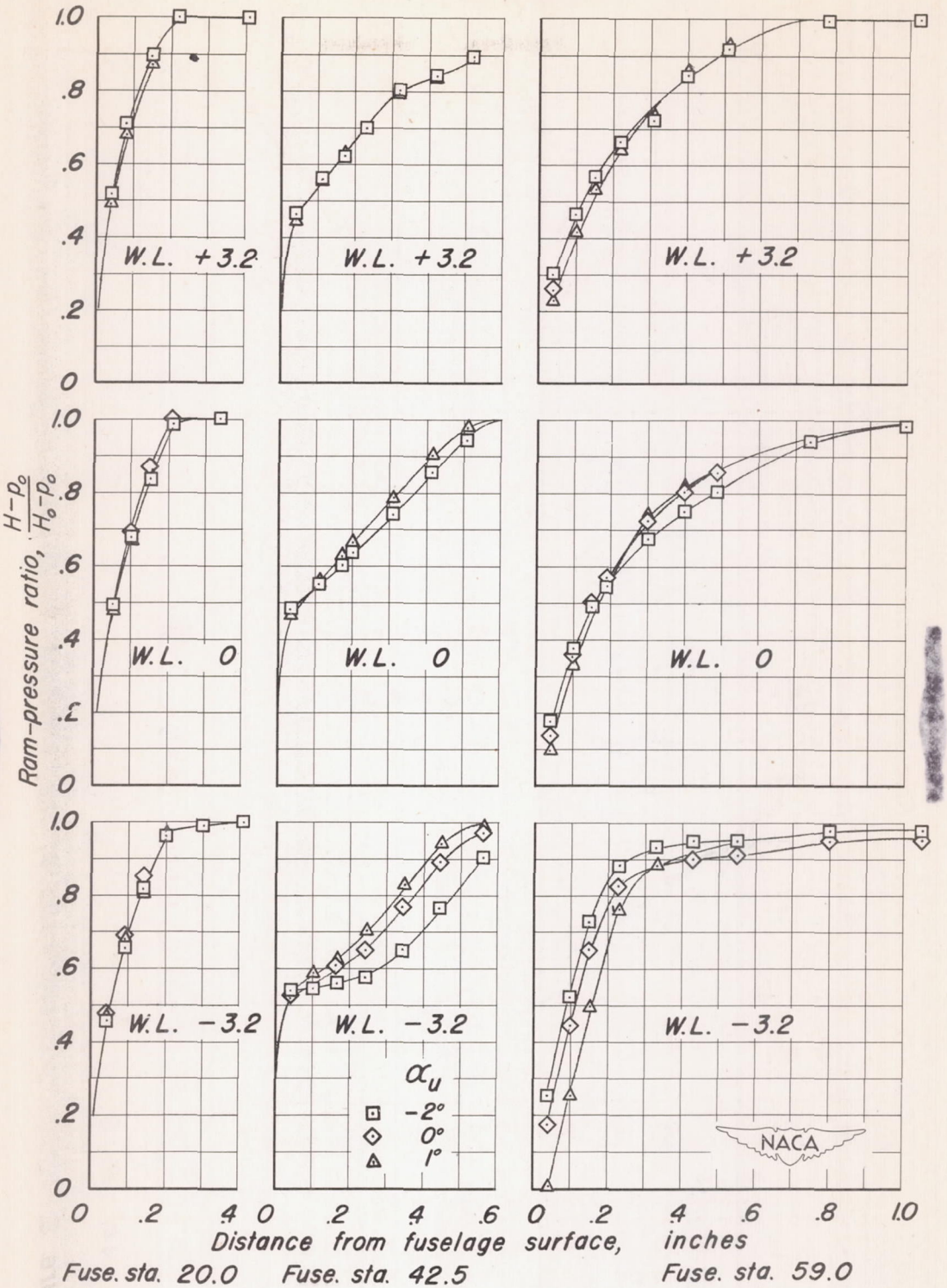

(e) M_0, 0.875

Figure 7.— Concluded.

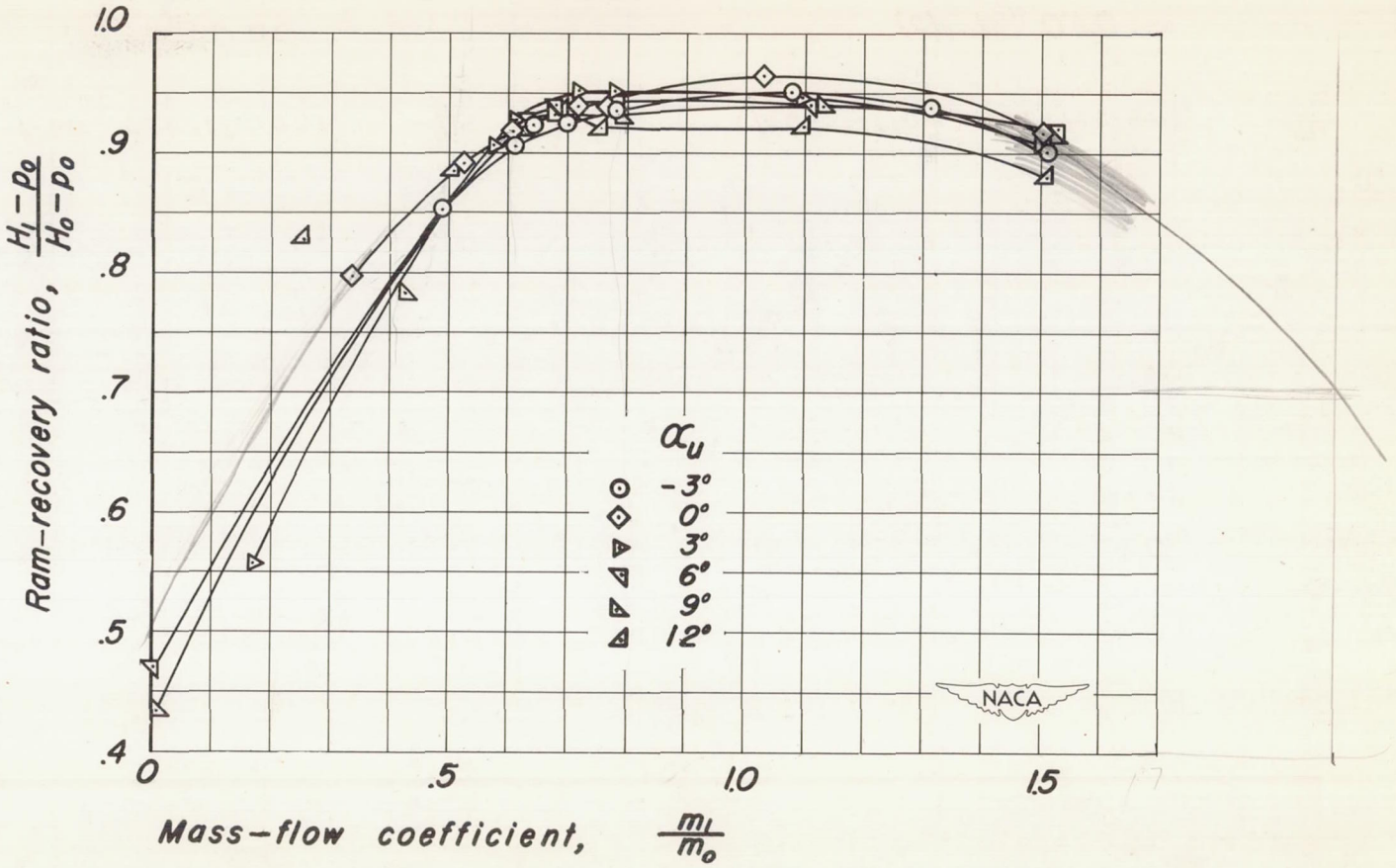

(a) M_0, 0.30

Figure 8. — Ram-recovery ratio at the entrance in relation to mass-flow coefficient.

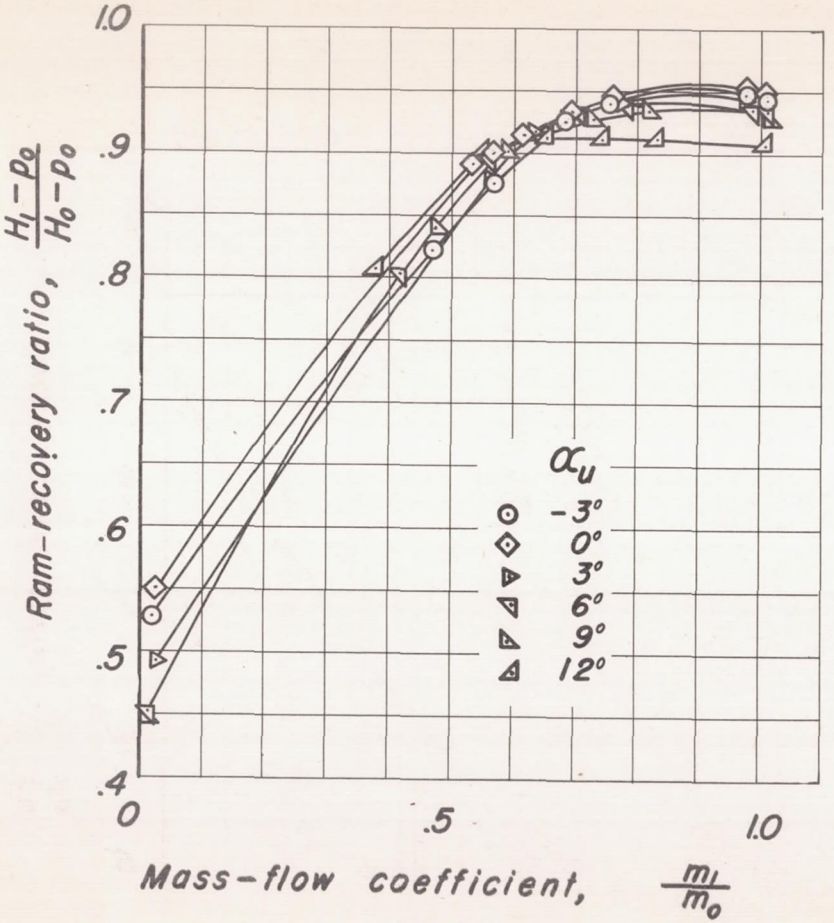

(b) M_0, 0.60

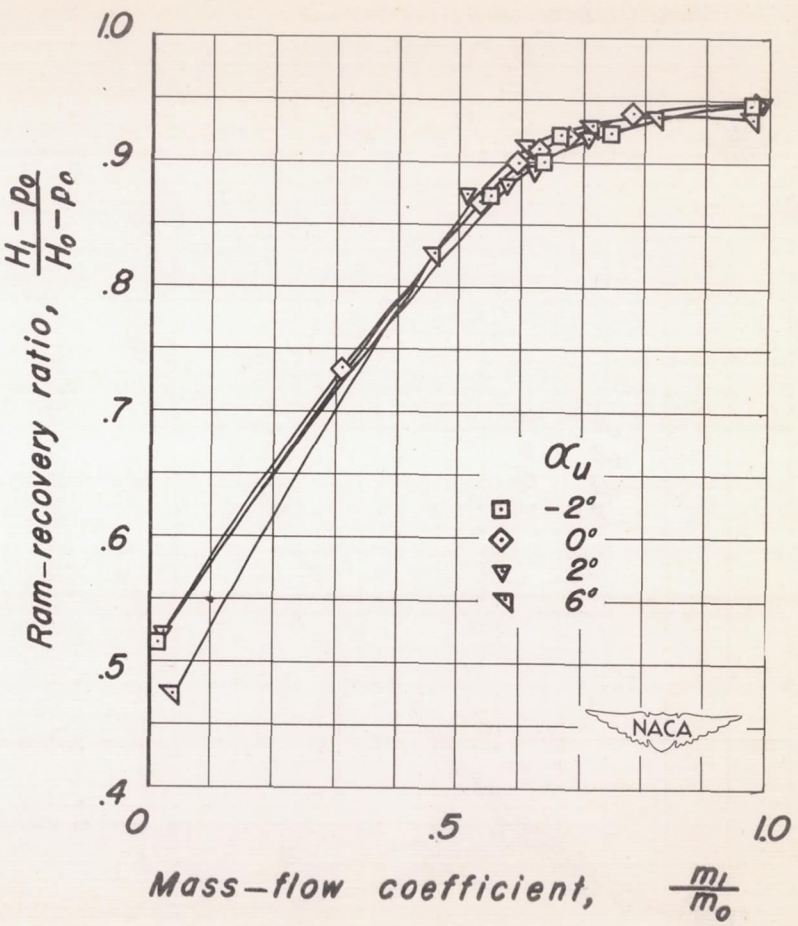

(c) M_0, 0.70

Figure 8. – Continued.

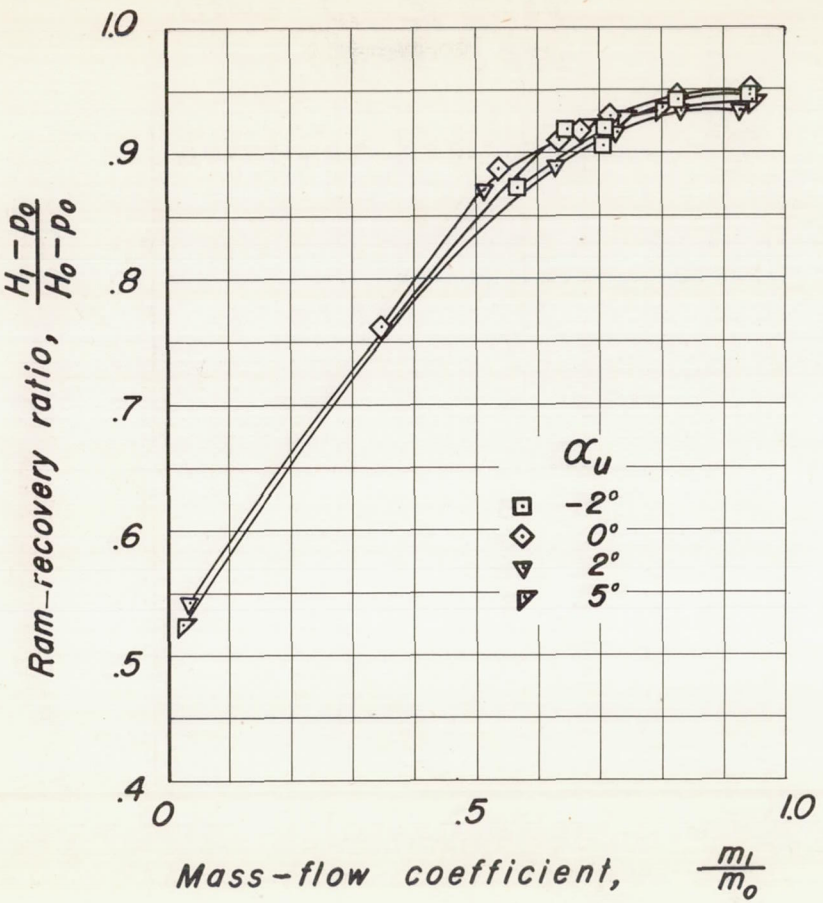

(d) M_0, 0.75

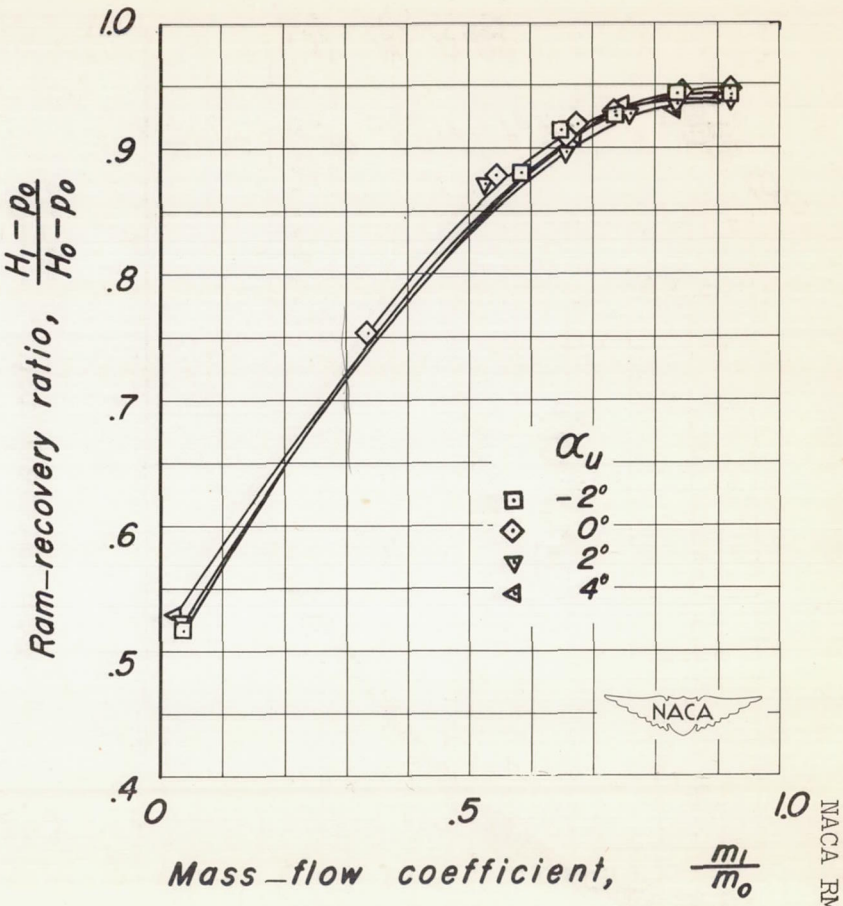

(e) M_0, 0.80

Figure 8. – Continued.

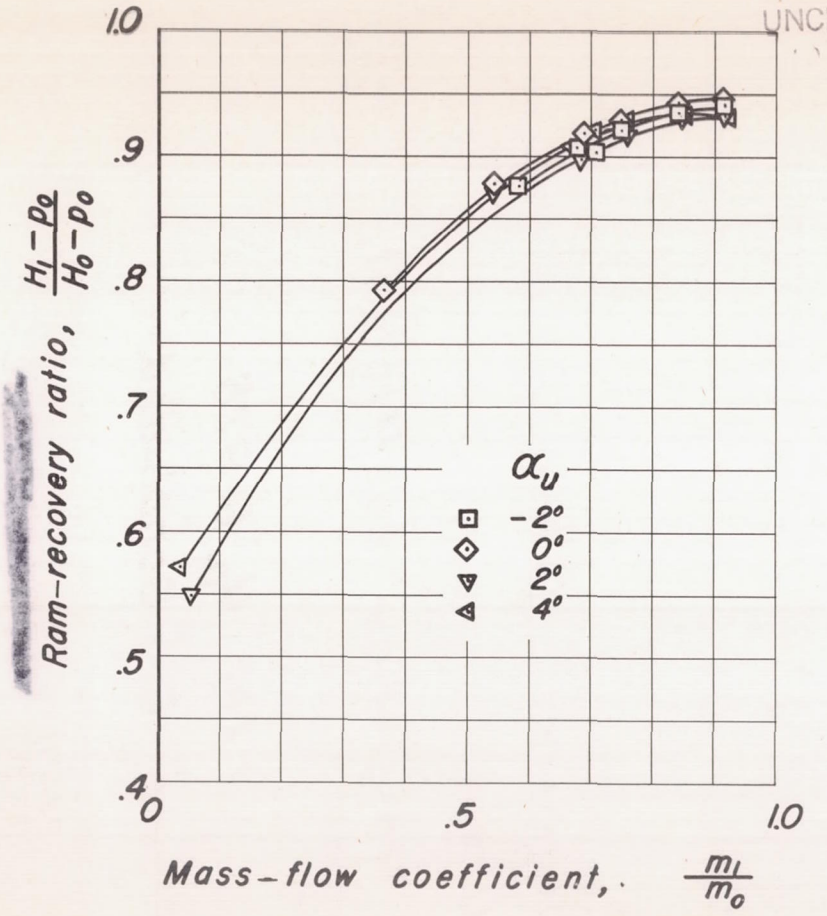

(f) M_0, 0.825

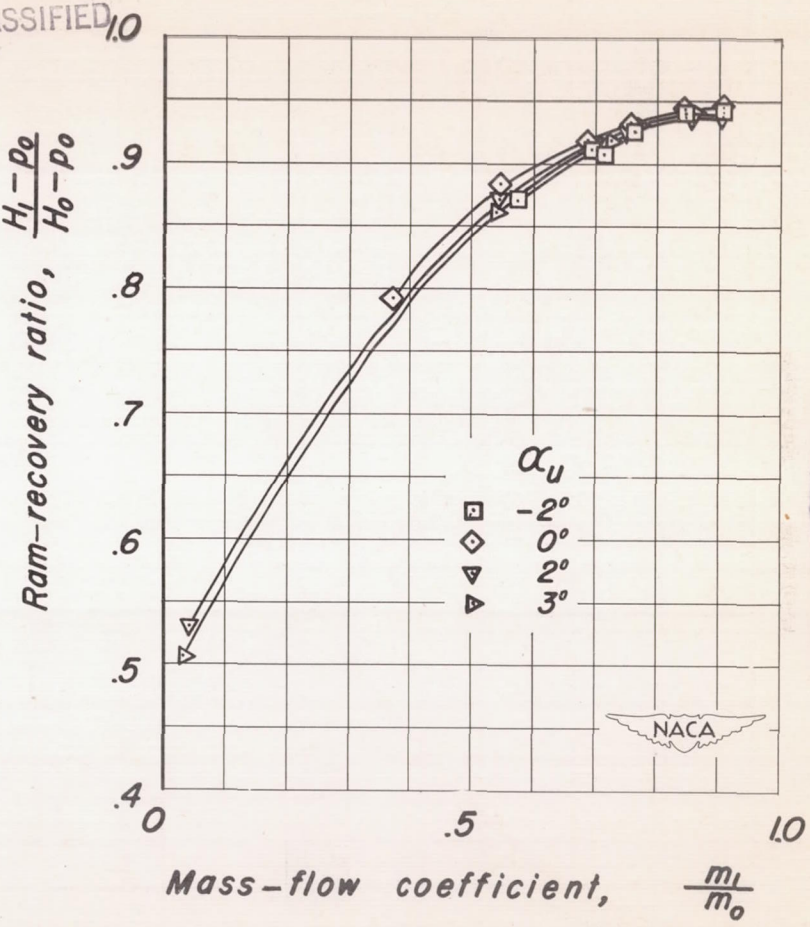

(g) M_0, 0.85

Figure 8. – Continued.

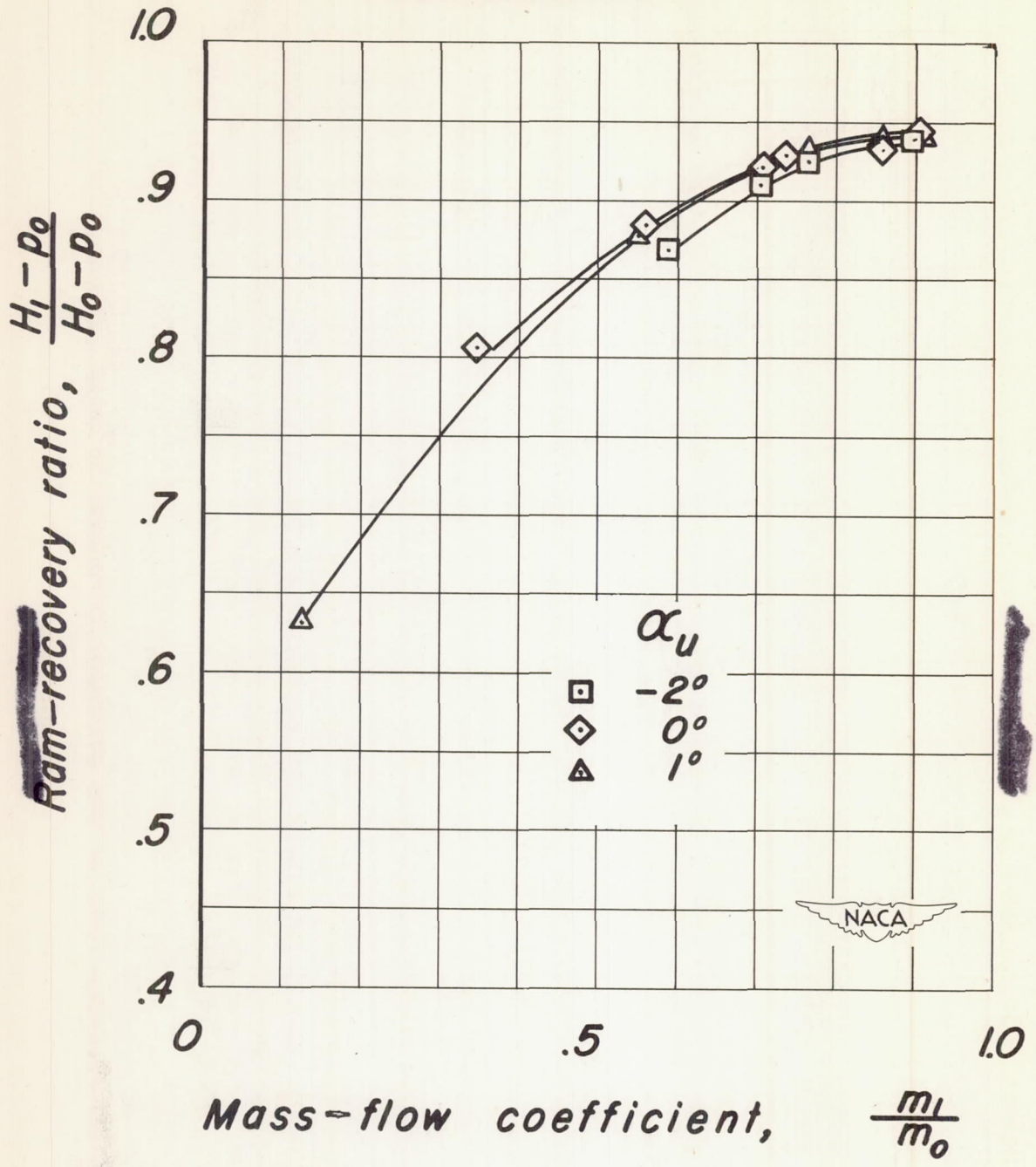

(h) M_0, 0.875

Figure 8. - Concluded.

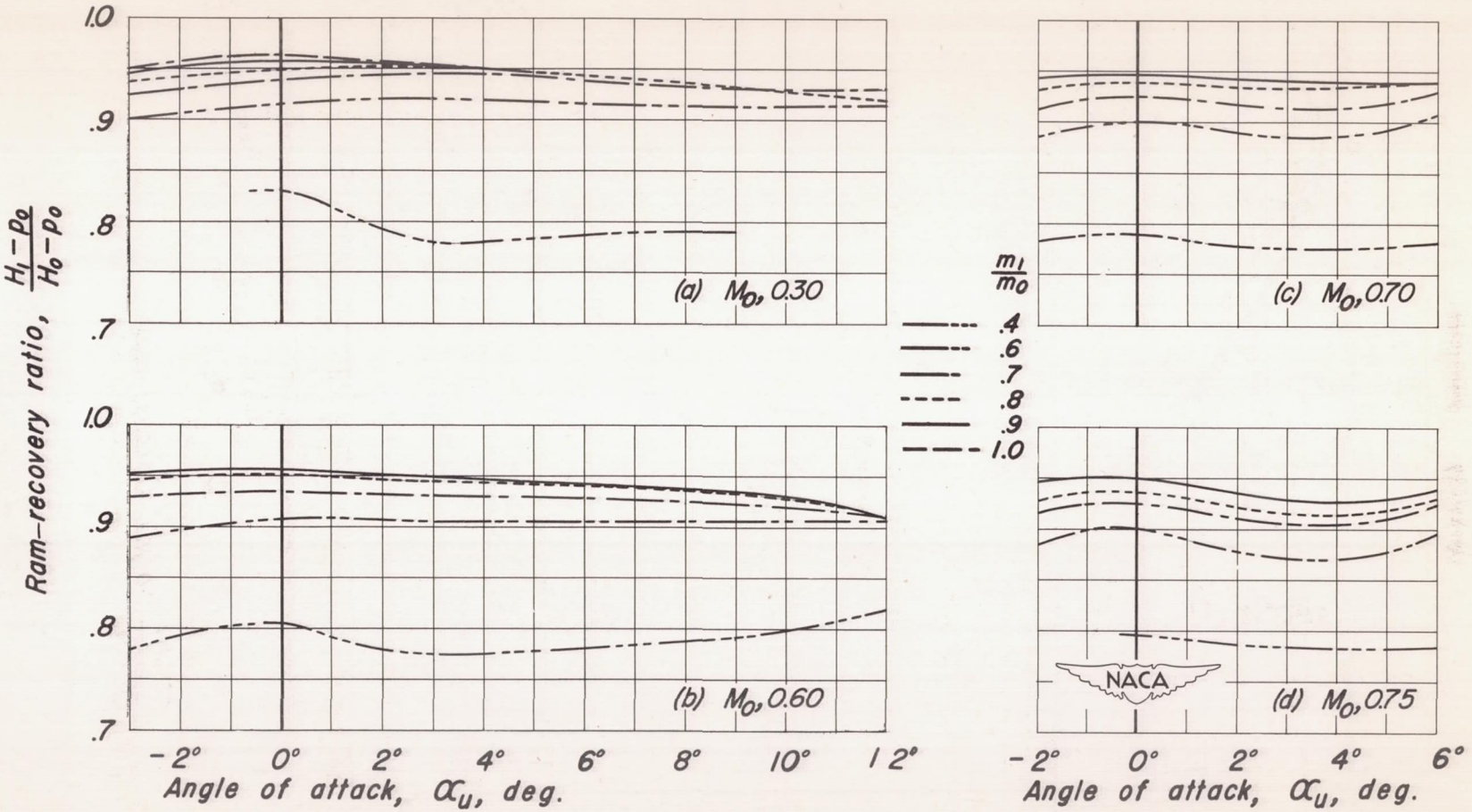

Figure 9.— Ram-recovery ratio at the entrance in relation to angle of attack.

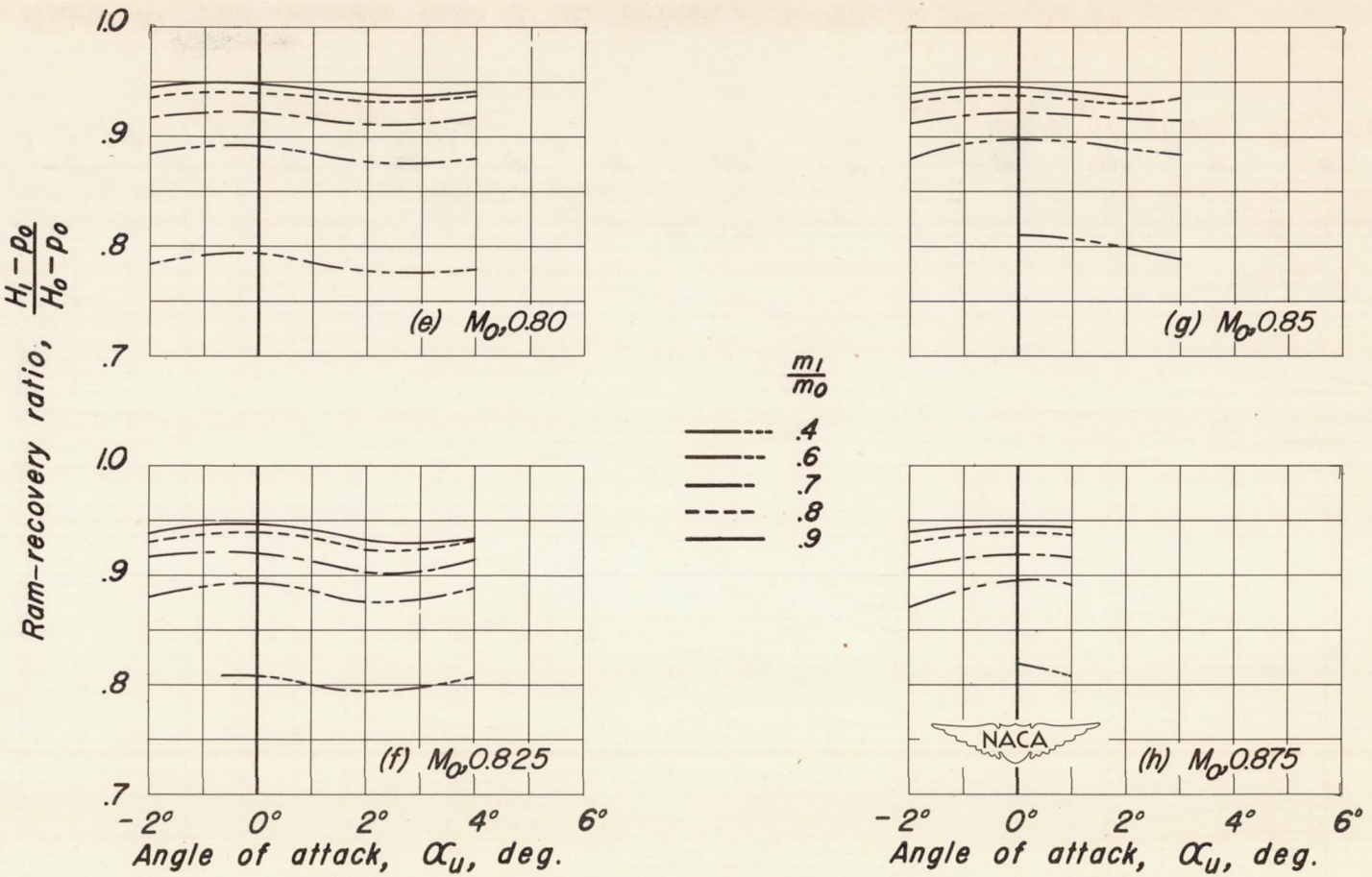

Figure 9. – Concluded.

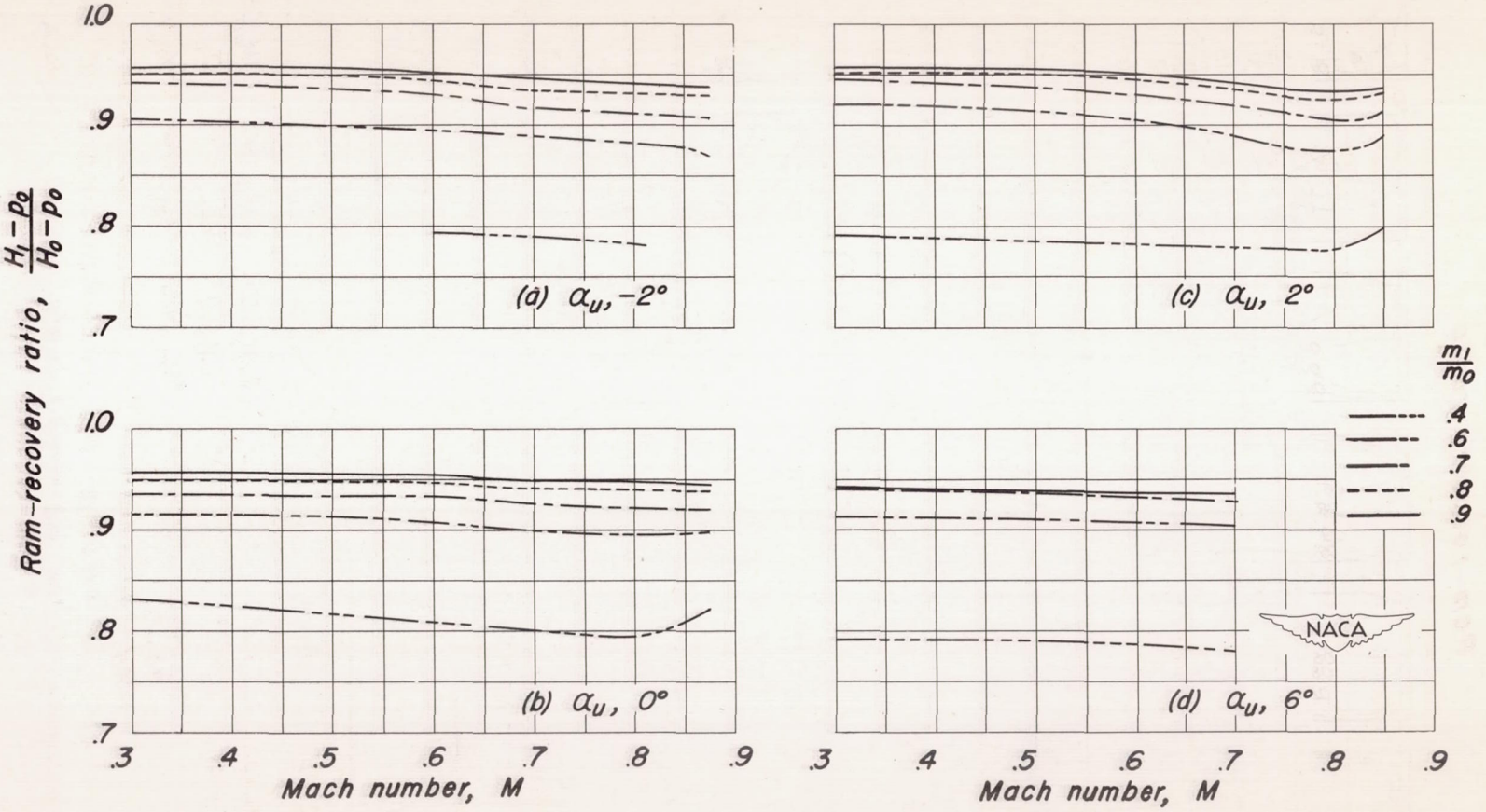

Figure 10.– Ram–recovery ratio at the entrance in relation to Mach number.

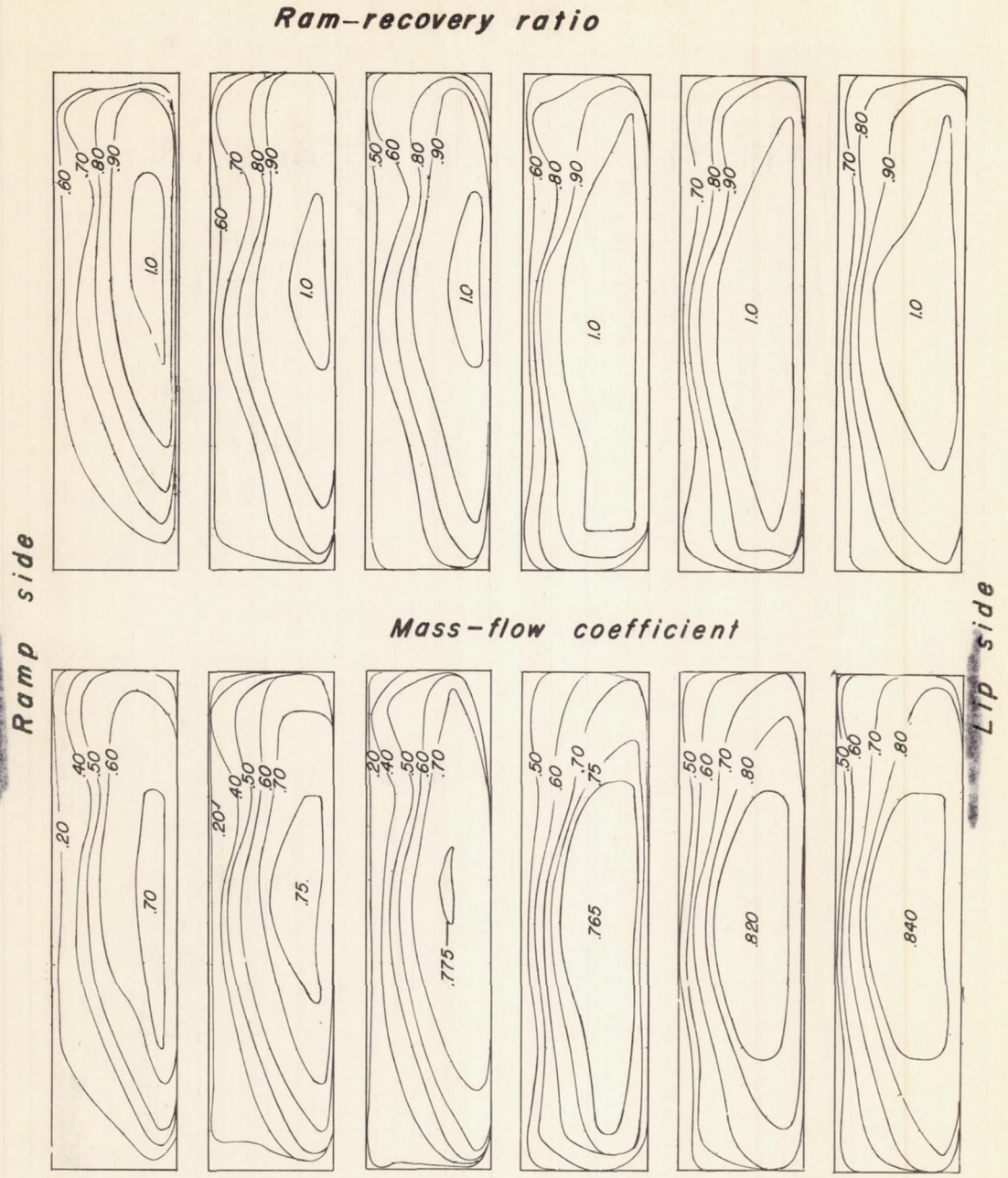

Figure 11.- Ram recovery and mass-flow contours at the entrance of the submerged inlets.

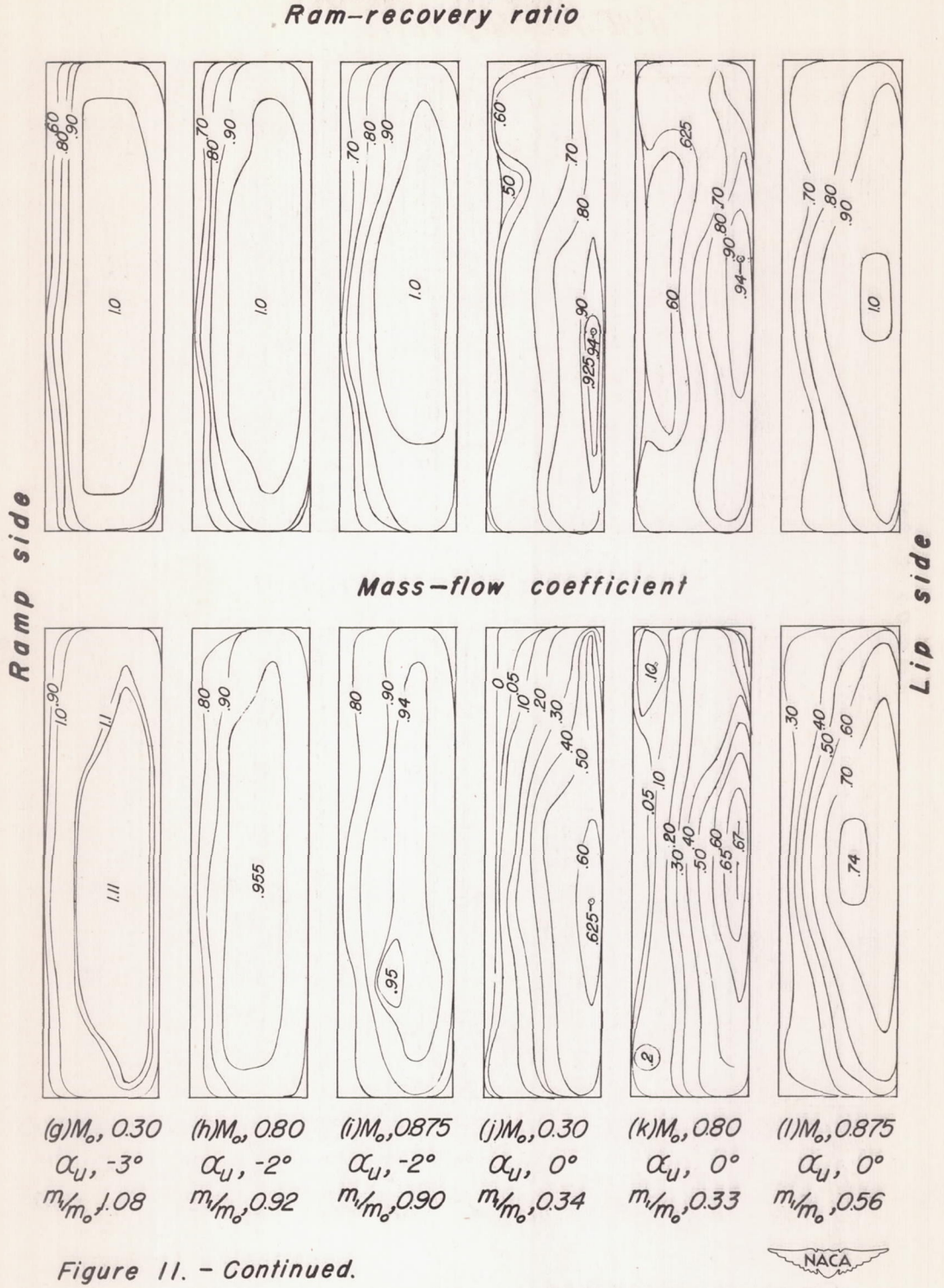

Figure 11. - Continued.

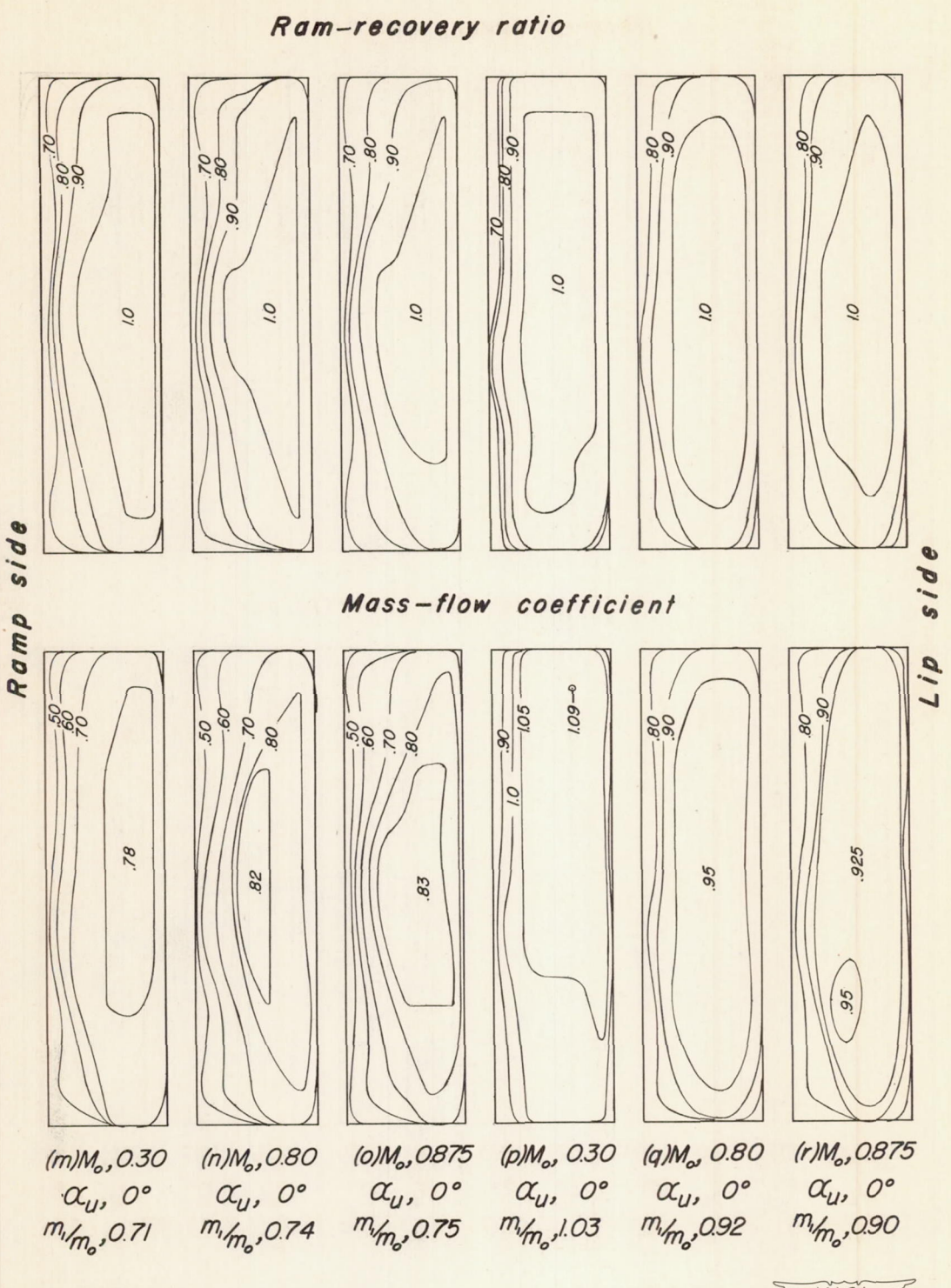

Figure 11. - Continued.

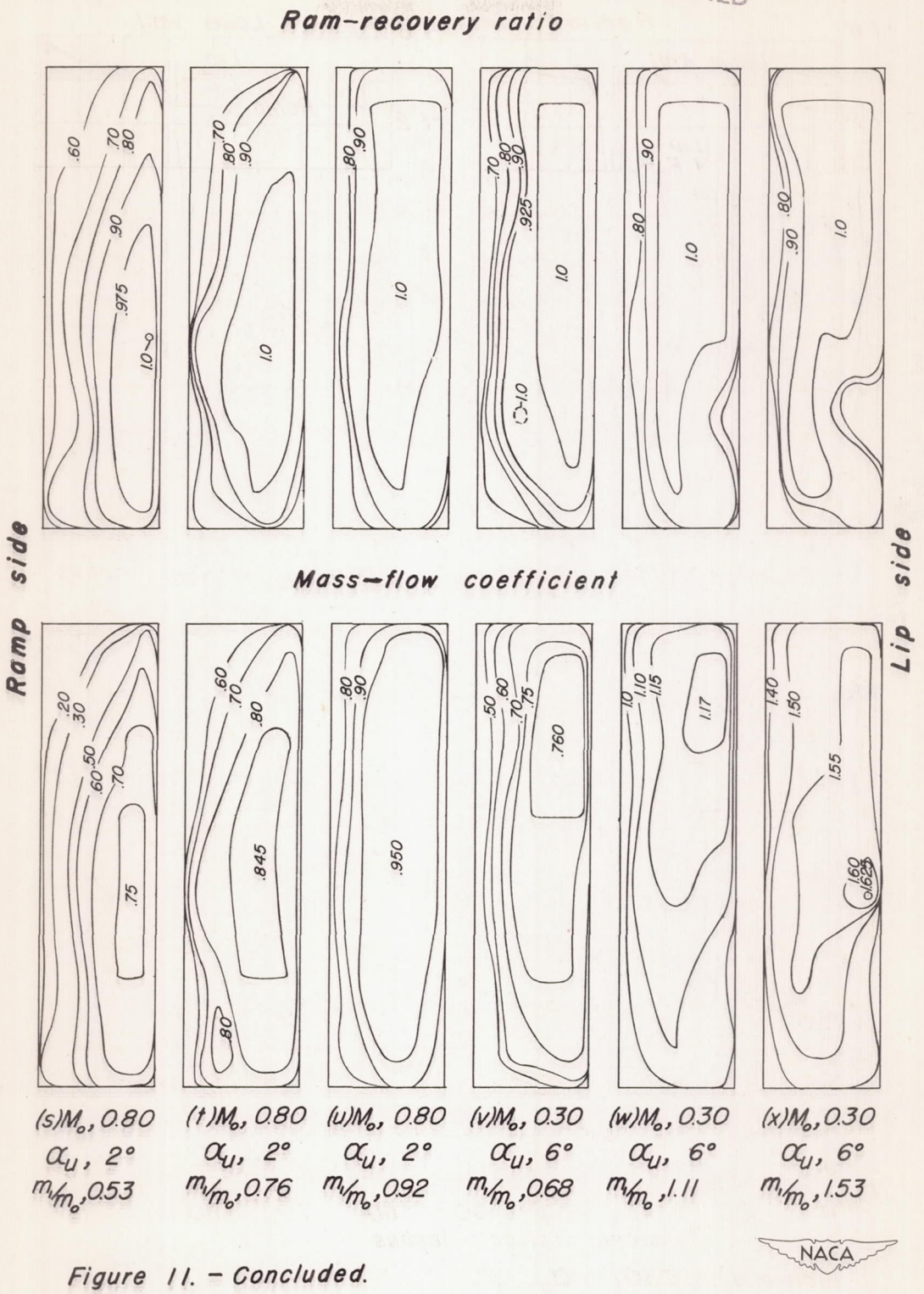

Figure 11. – Concluded.

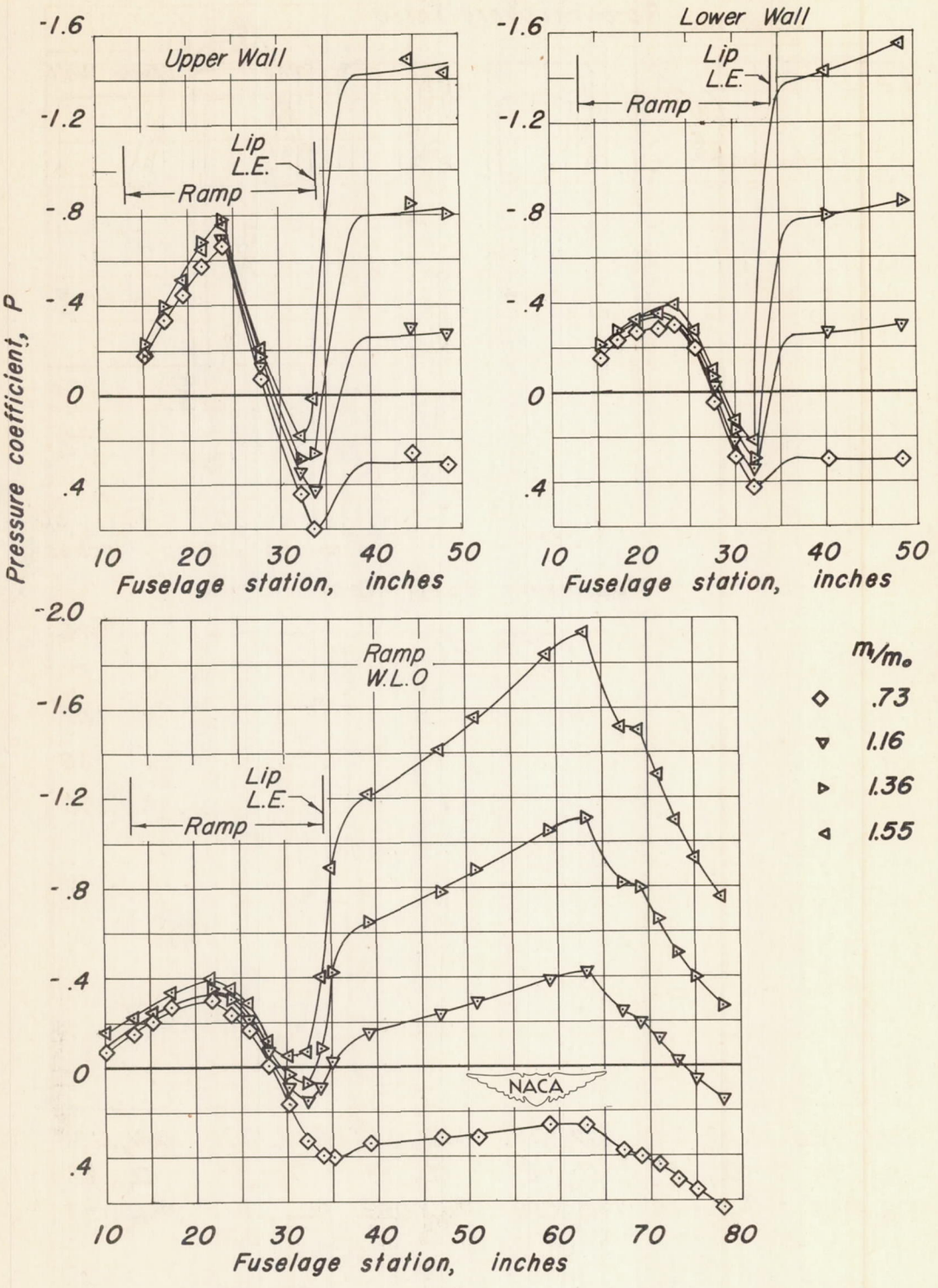

(a) M_0 0.30; α_u, -3°.

Figure 12.- Pressure distribution along the ramp and inside the duct.

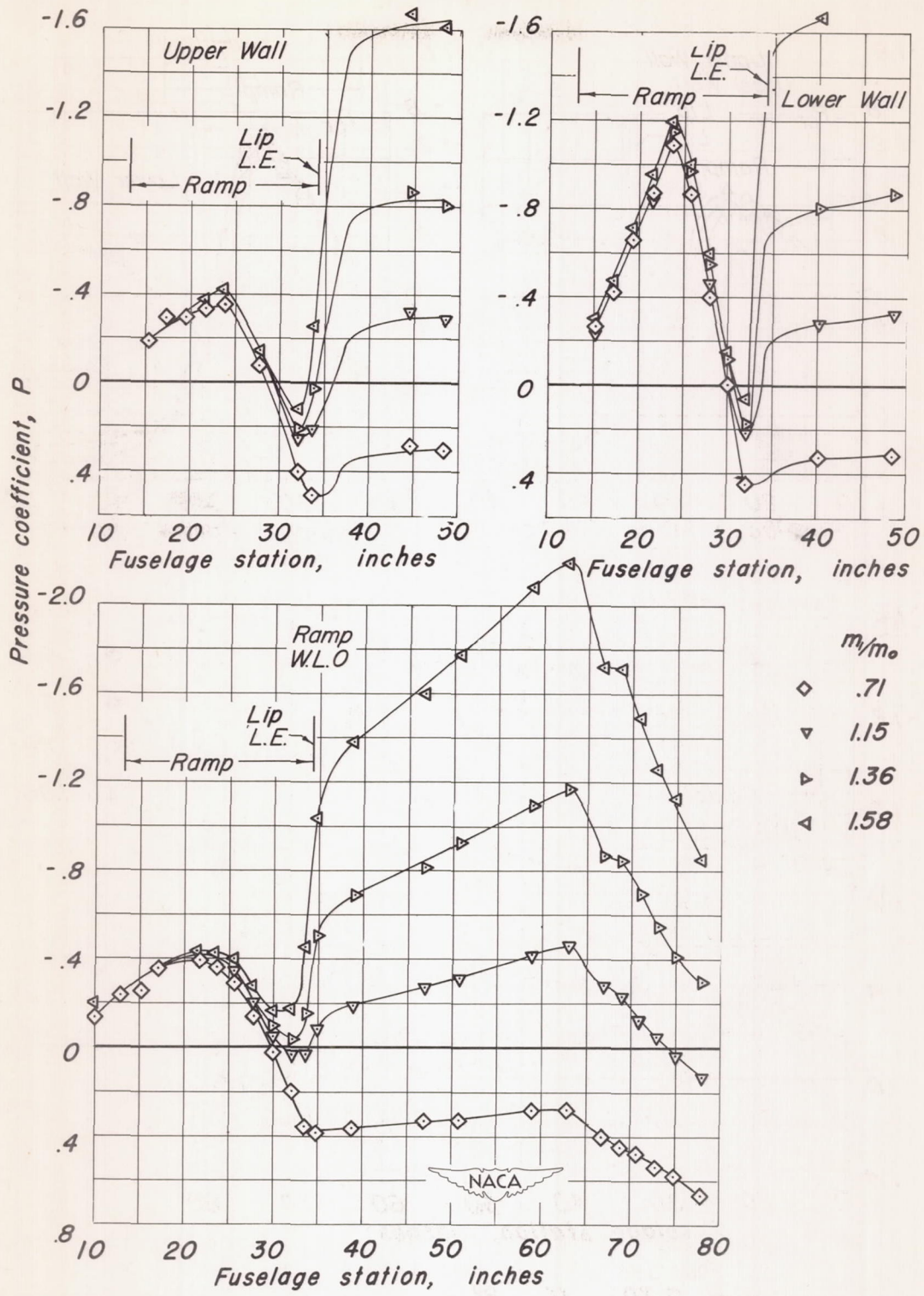

(b) M_0, 0.30; α_u, 6°.

Figure 12. – Continued.

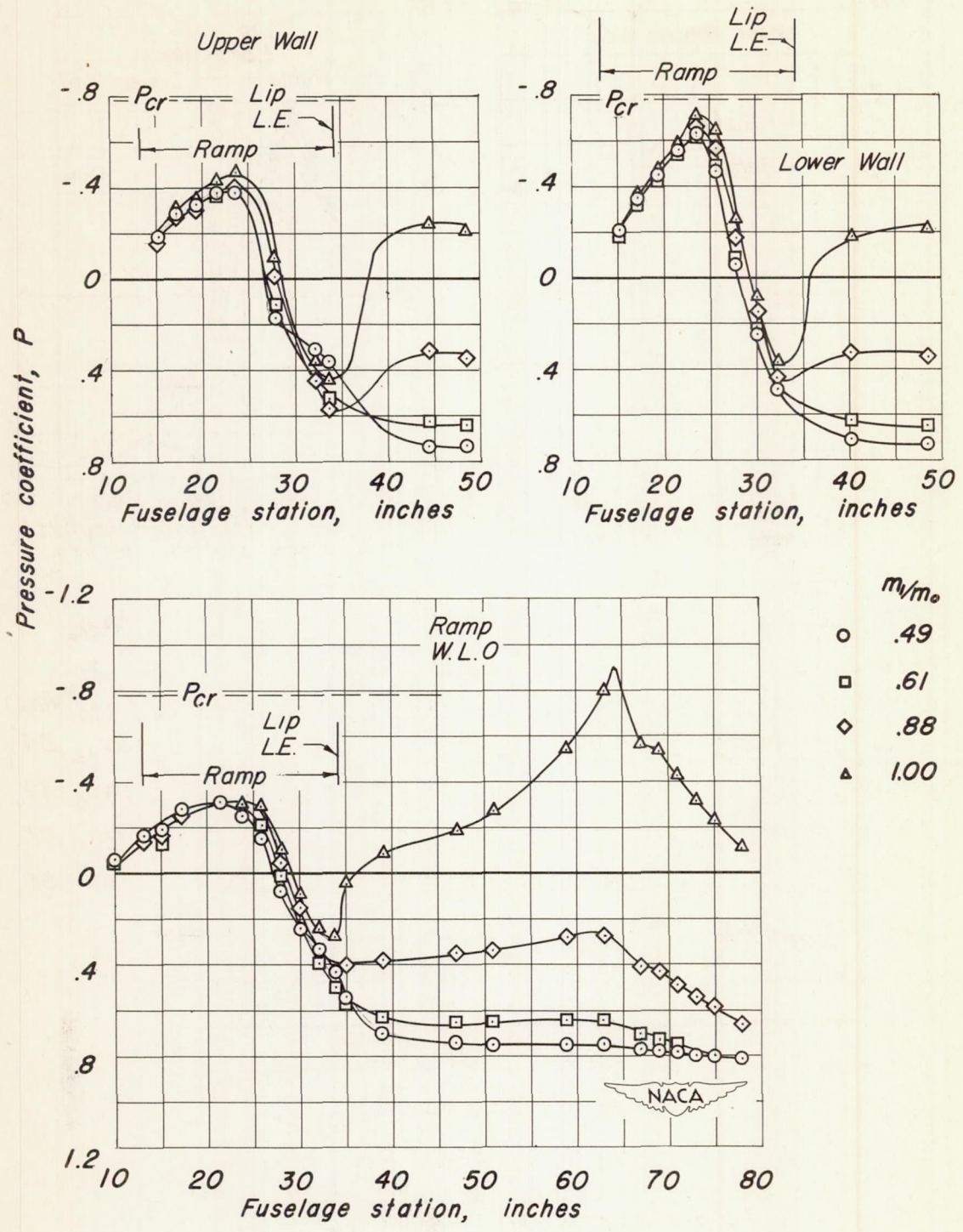

(c) M_0, 0.70; α_u, 2°.

Figure 12. – Continued.

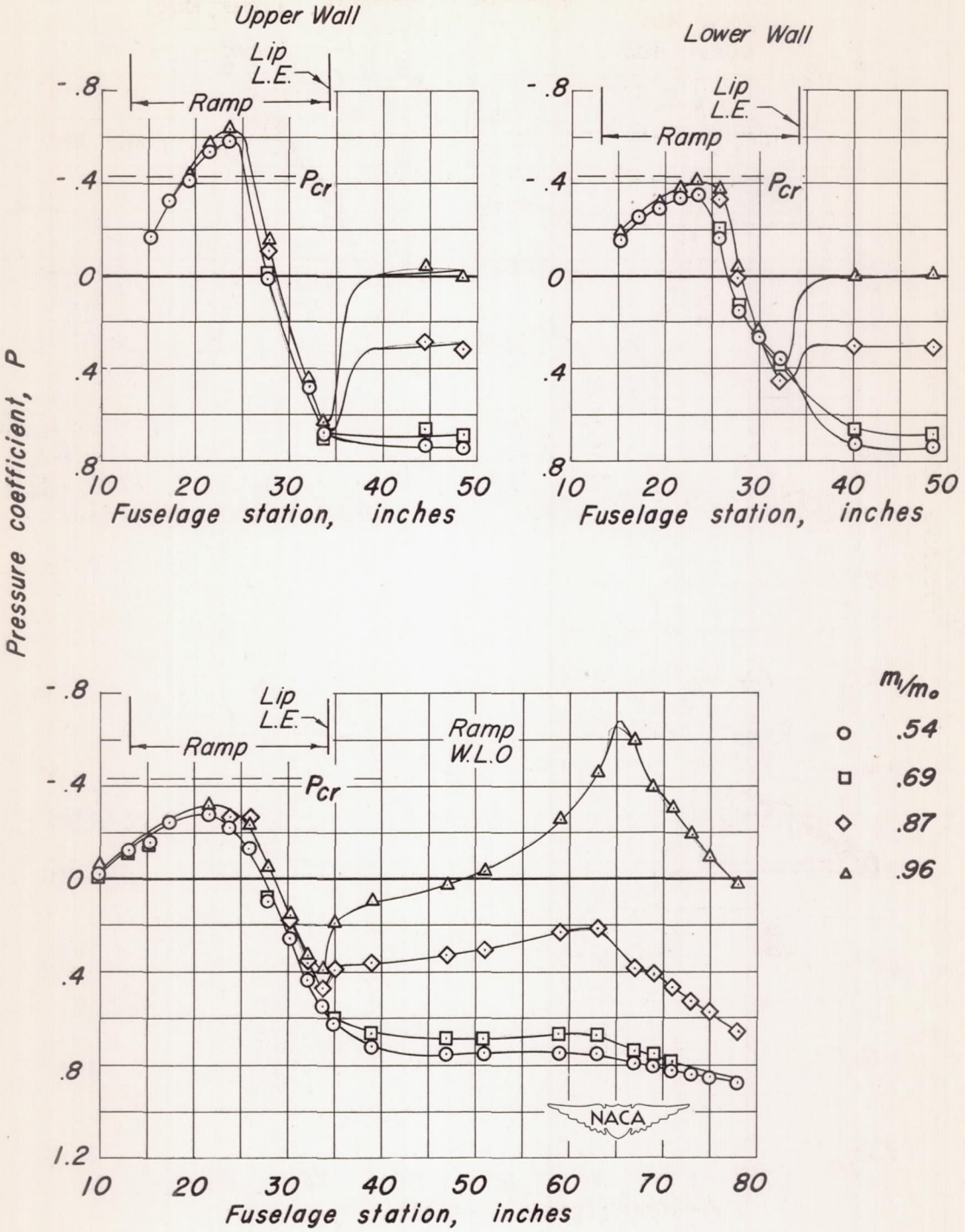

(d) M_o, 0.80; α_u, -2°

Figure 12.- Continued.

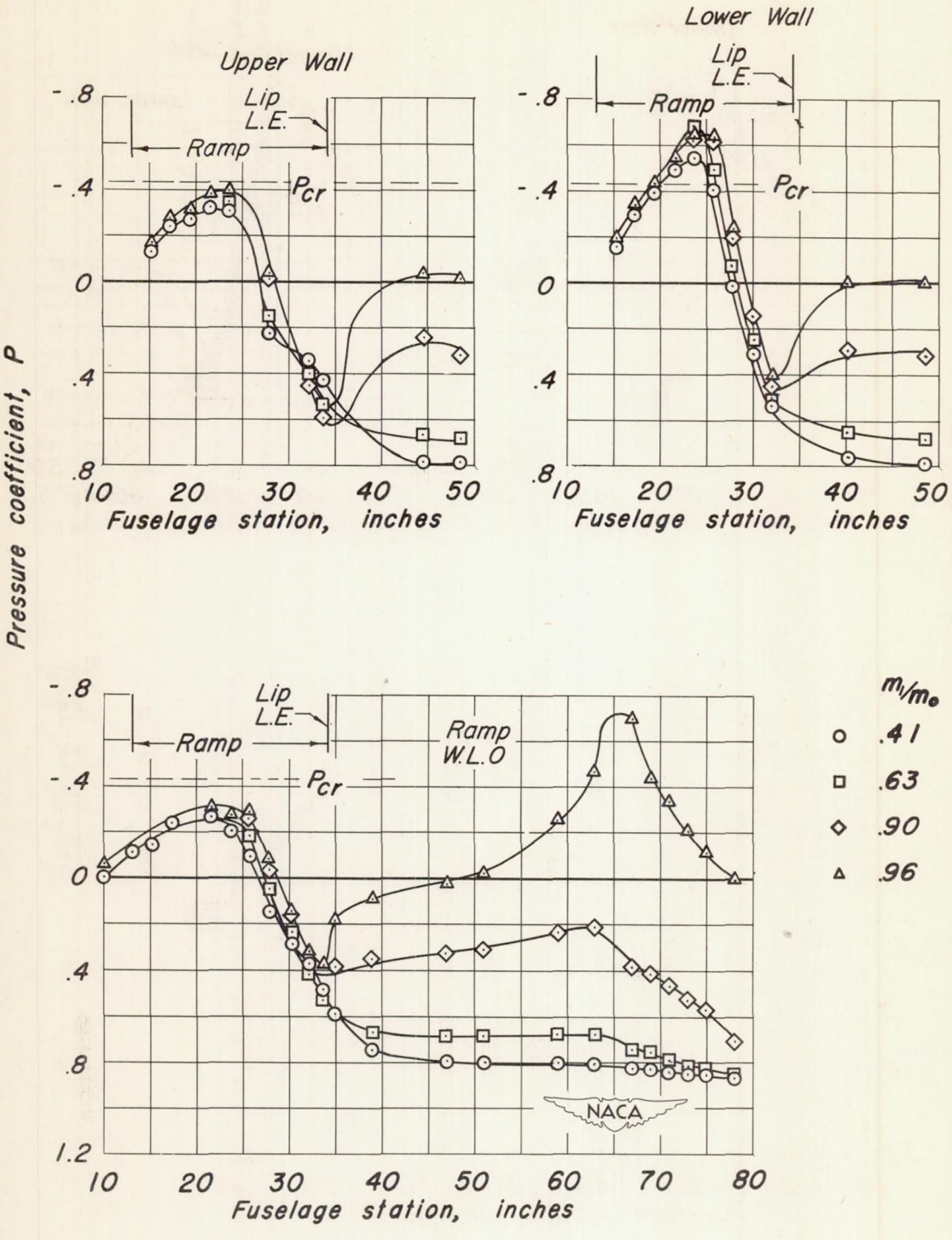

(e) M_0, 0.80; α_u, 2°.

Figure 12. – Continued.

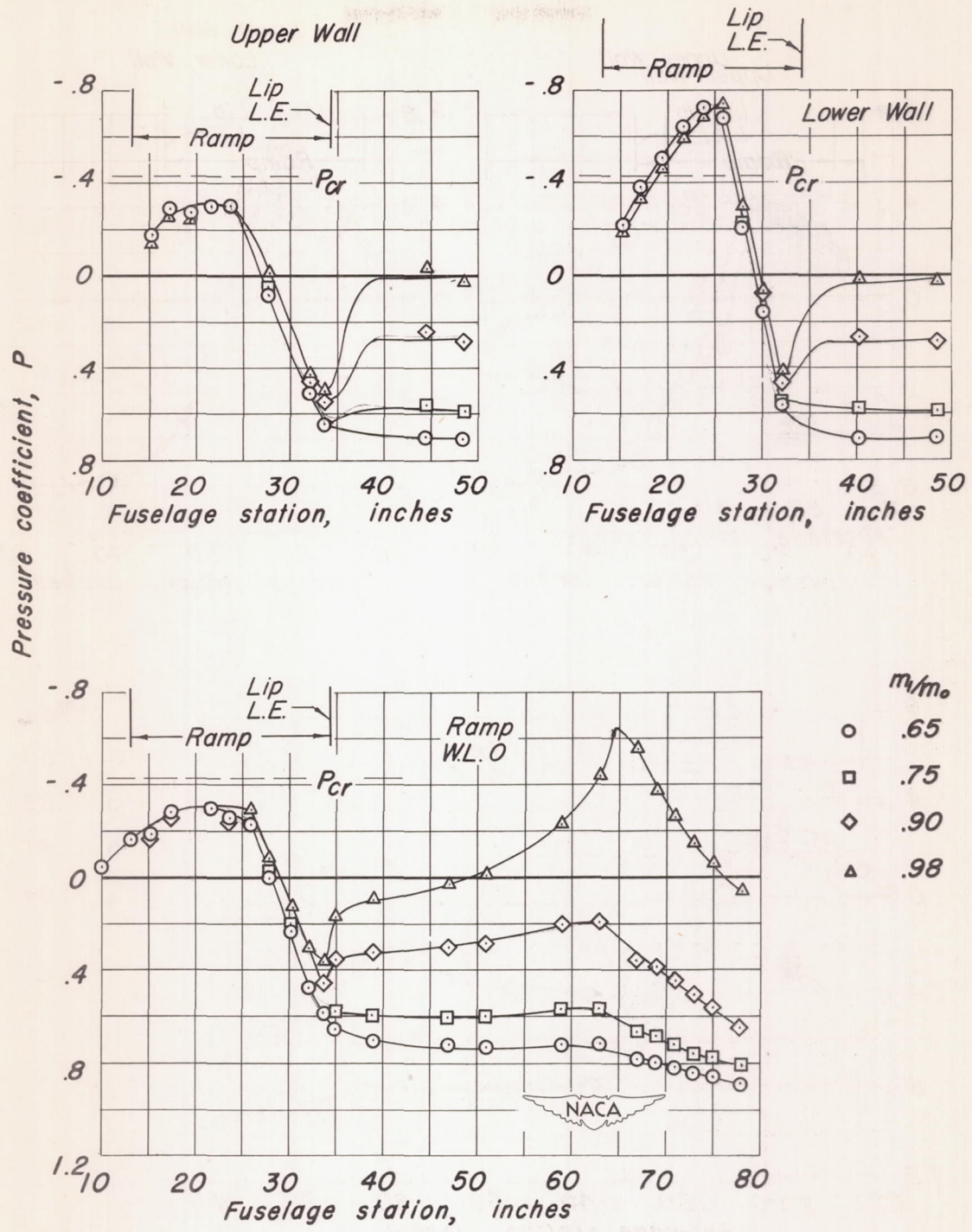

(f) M_0, 0.80; α_u, 4°.

Figure 12. – Continued.

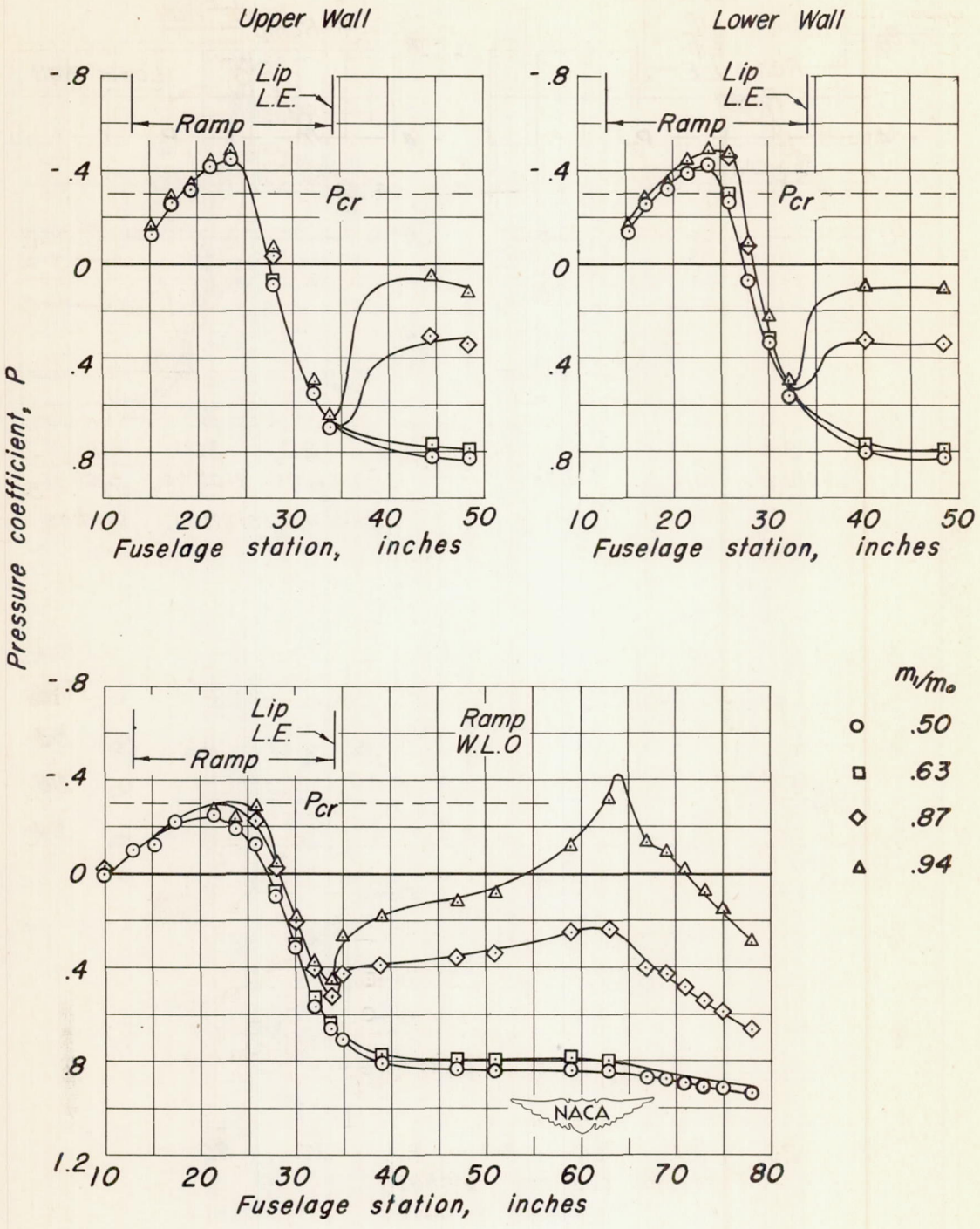

(g) M_0, 0.85; α_u, 0°.

Figure 12. – Continued.

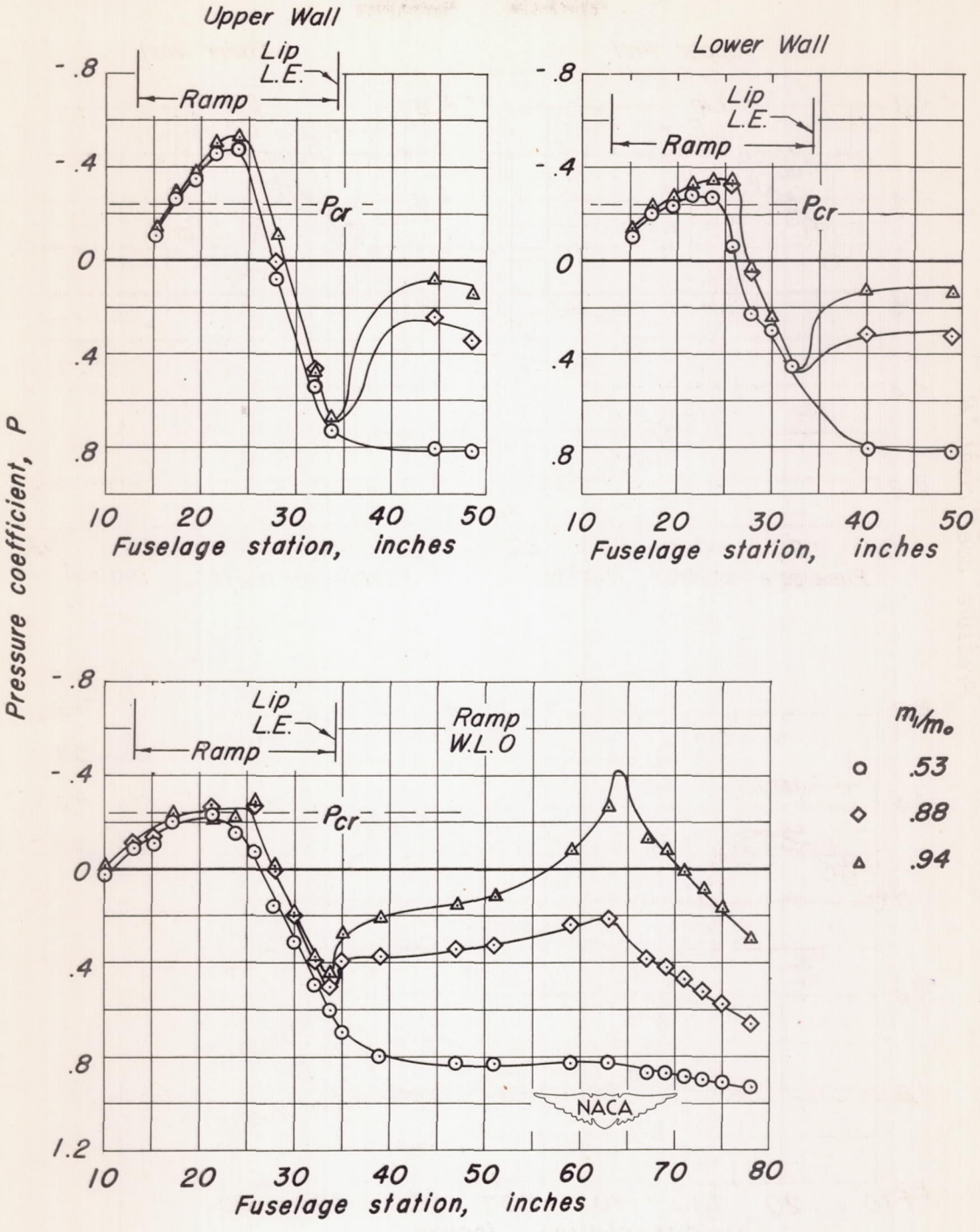

(h) M_o, 0.875; α_u, -2°.

Figure 12. – Continued.

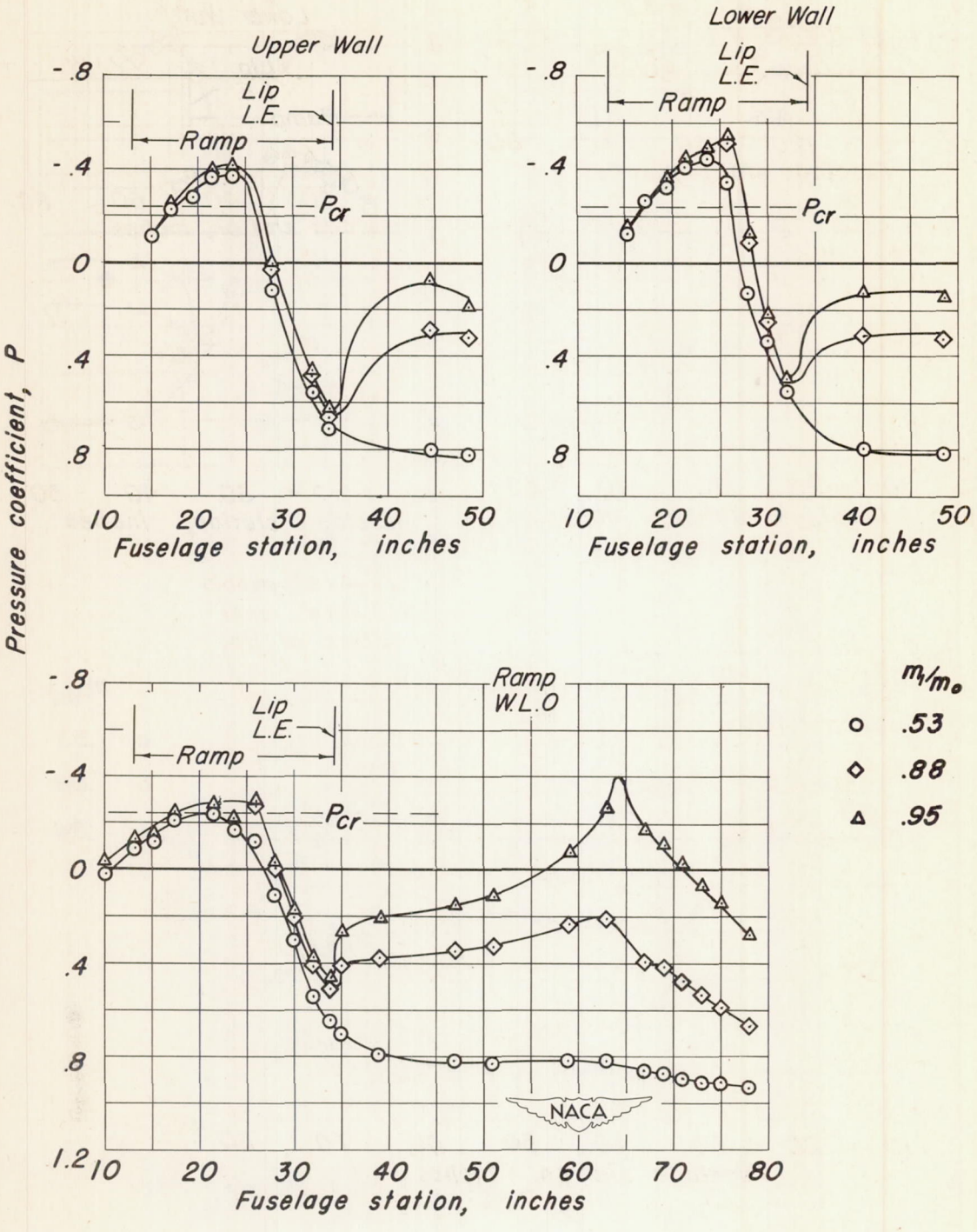

(i) M_o, 0.875; α_u, 1°

Figure 12. – Concluded.

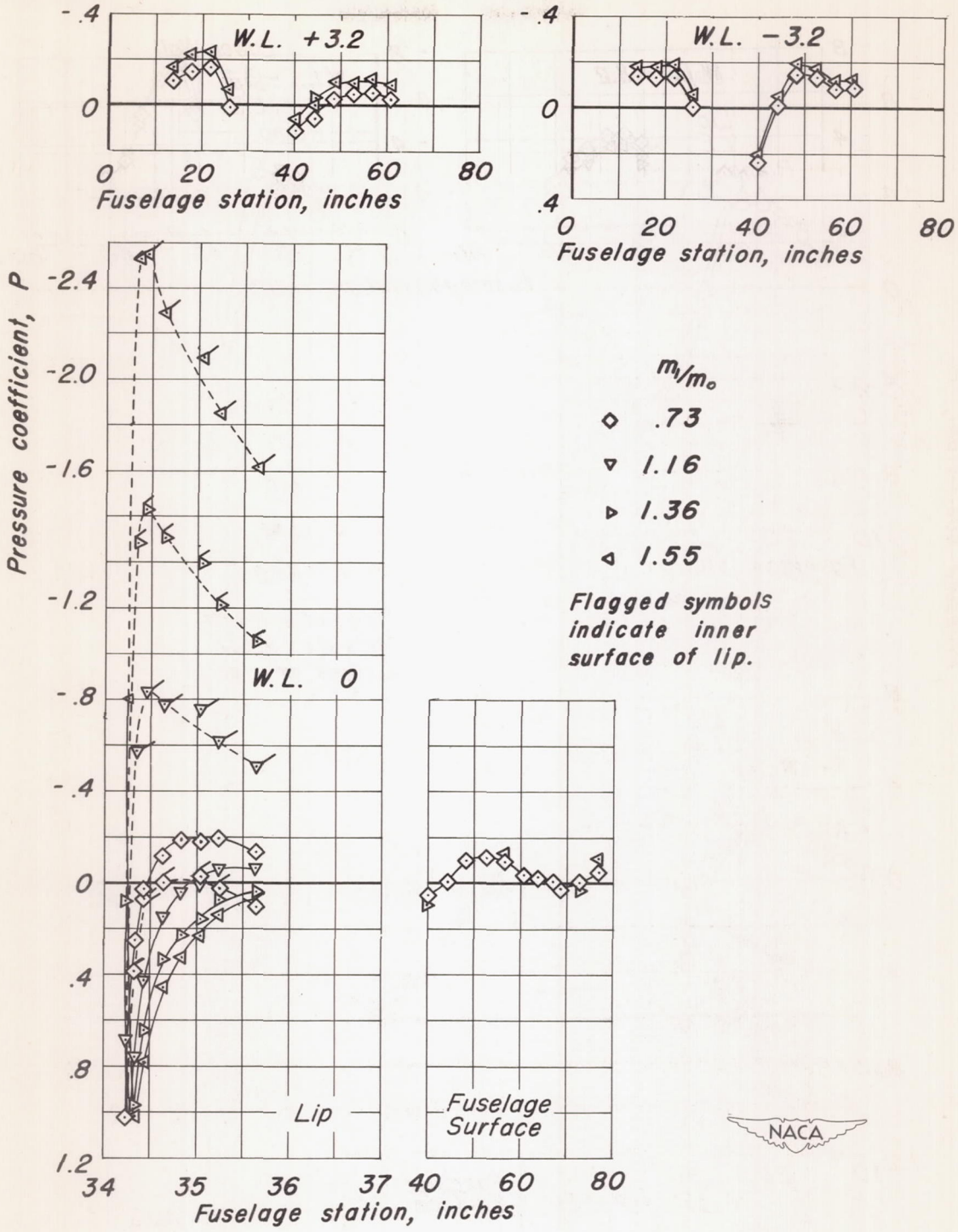

(a) M_0,0.30; α_u, -3°.

Figure 13.- Pressure distribution on inner and outer surface of lip and on fuselage surface adjacent to ramp.

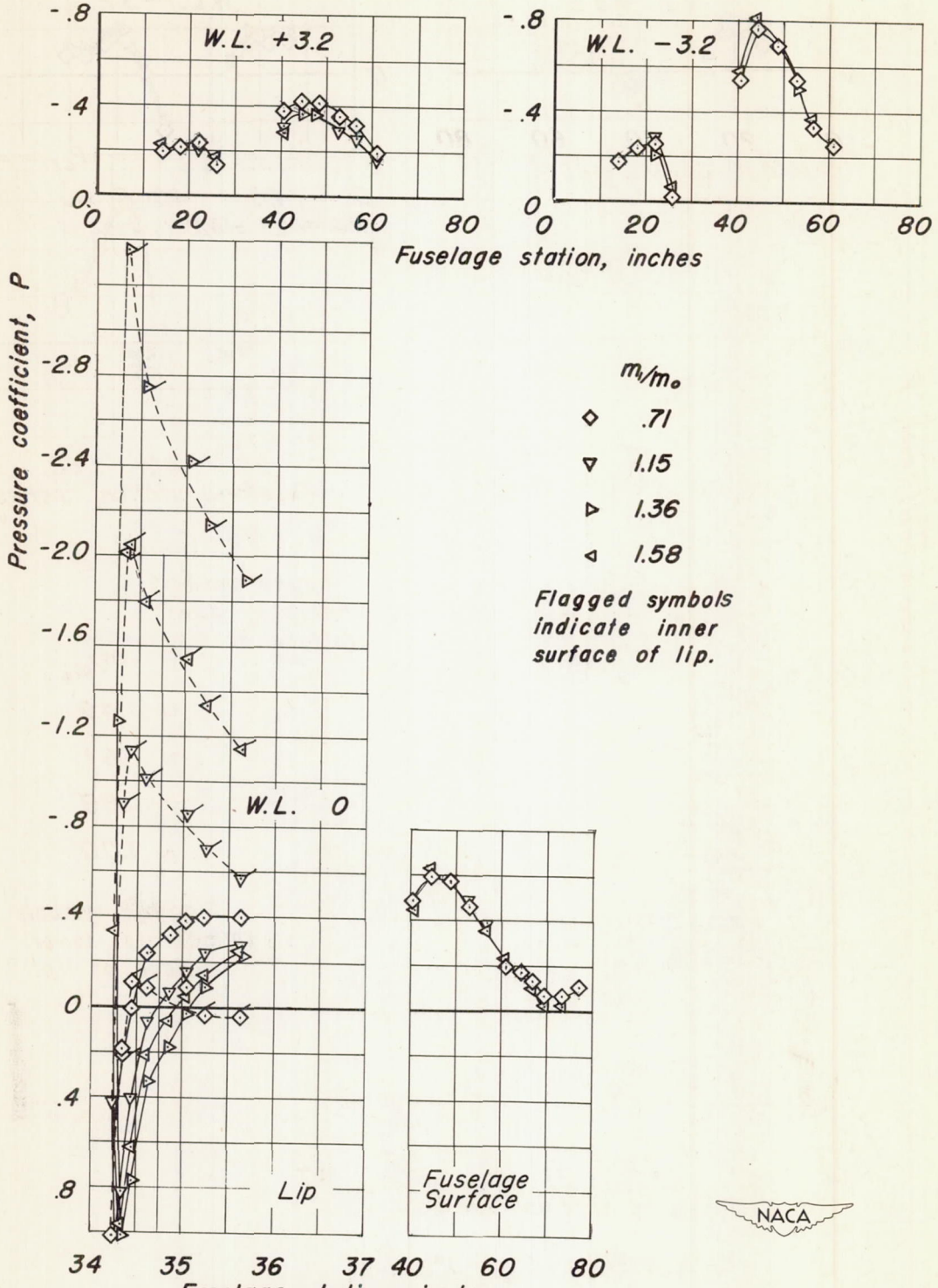

(b) M_∞ 0.30; α_u, 6°

Figure 13. – Continued.

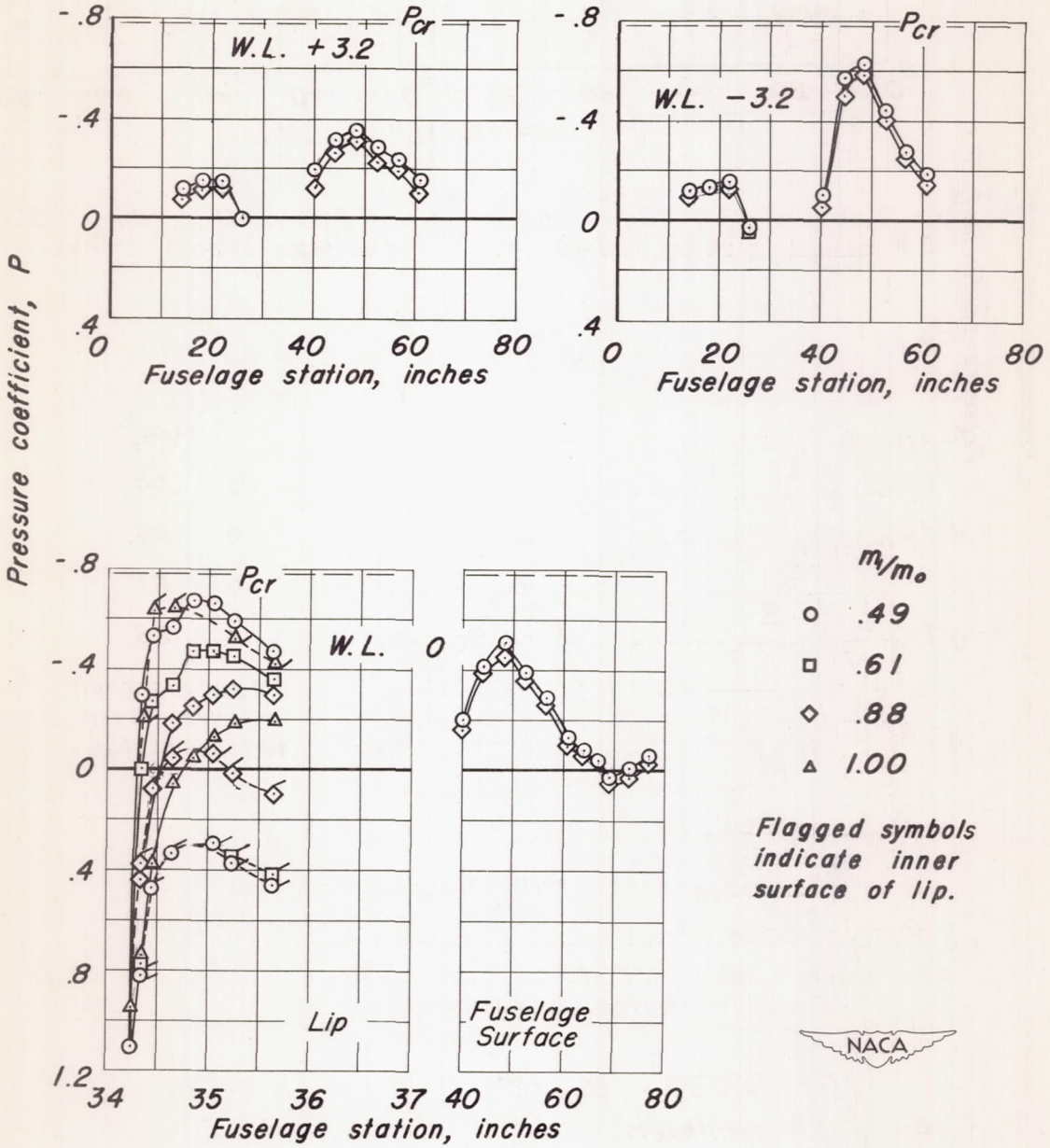

(c) M_o, 0.70; α_u, 2°.

Figure 13. – Continued.

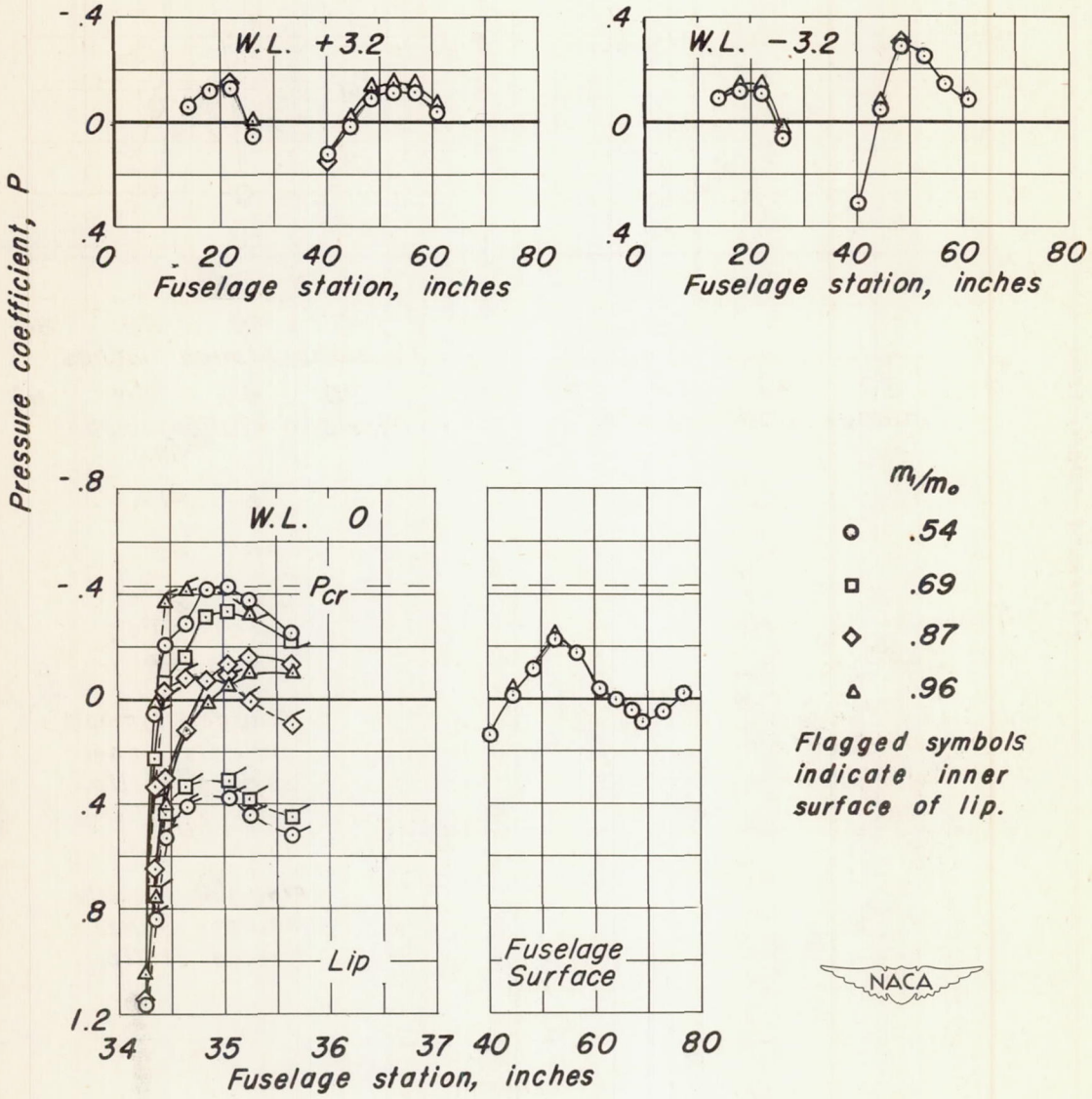

(d) M_o, 0.80; α_u, -2°.

Figure 13. – Continued.

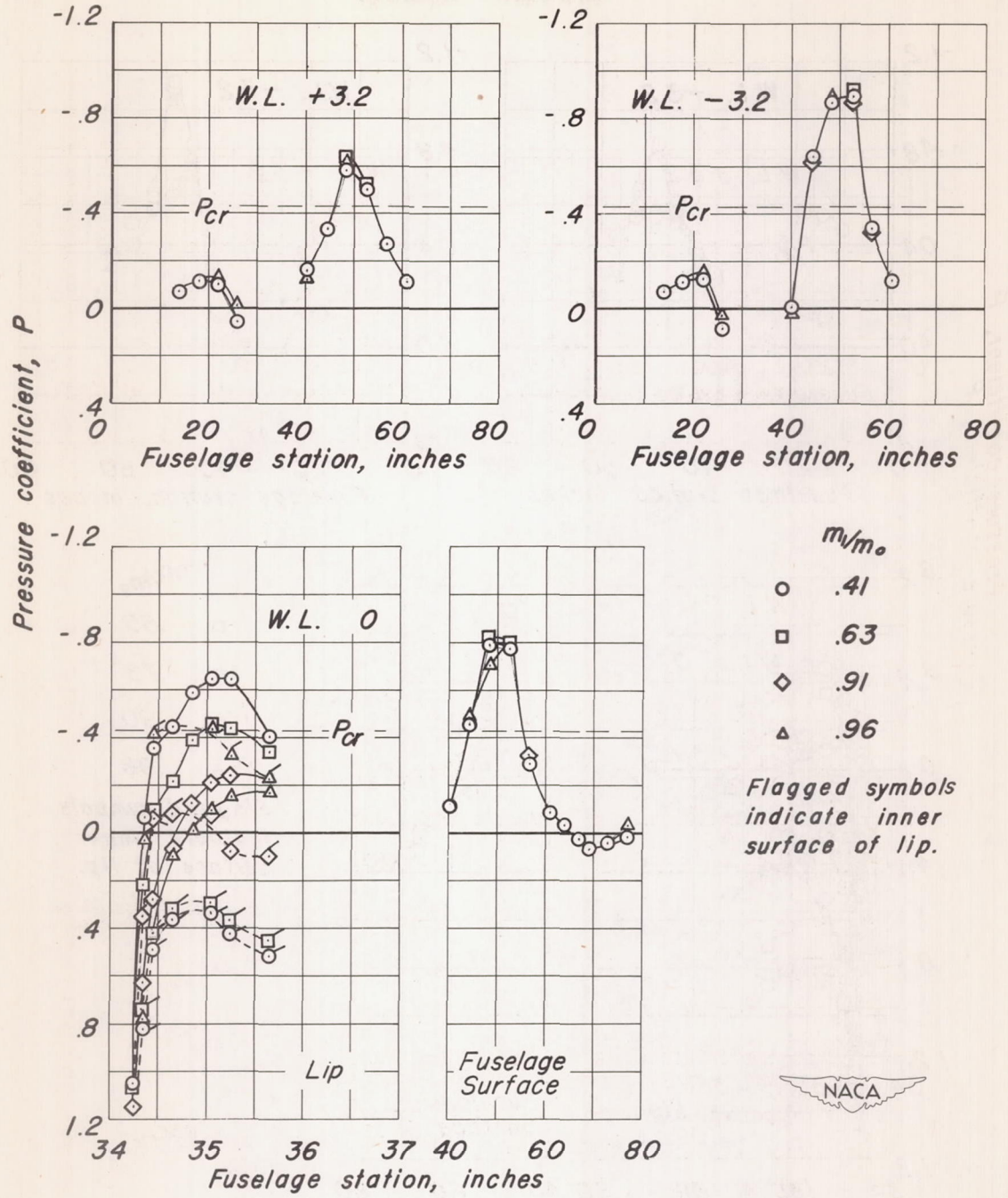

(e) M_o, 0.80; α_u, 2°.

Figure 13. – Continued.

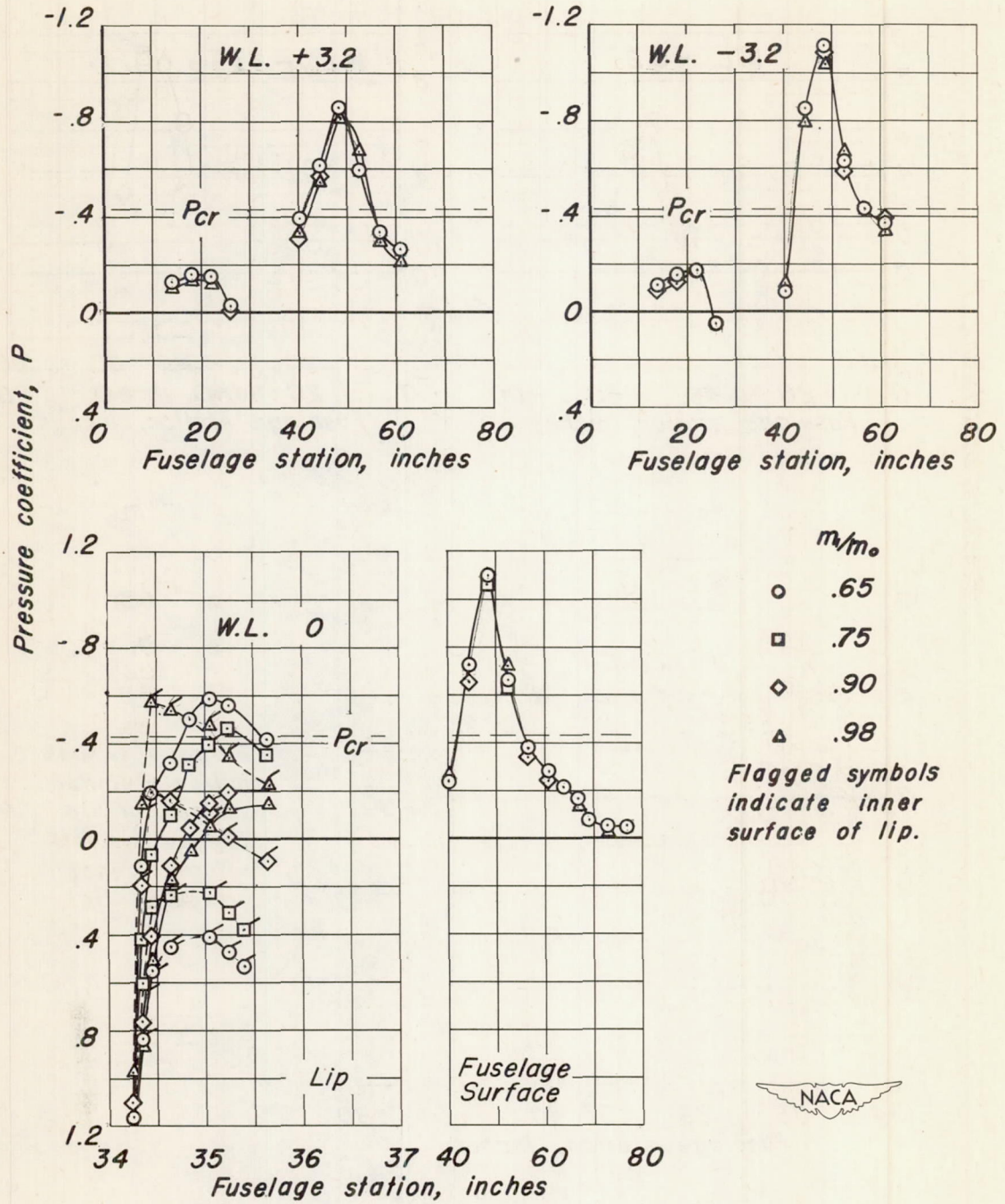

(f) M_o, 0.80; α_u, 4°

Figure 13. – Continued.

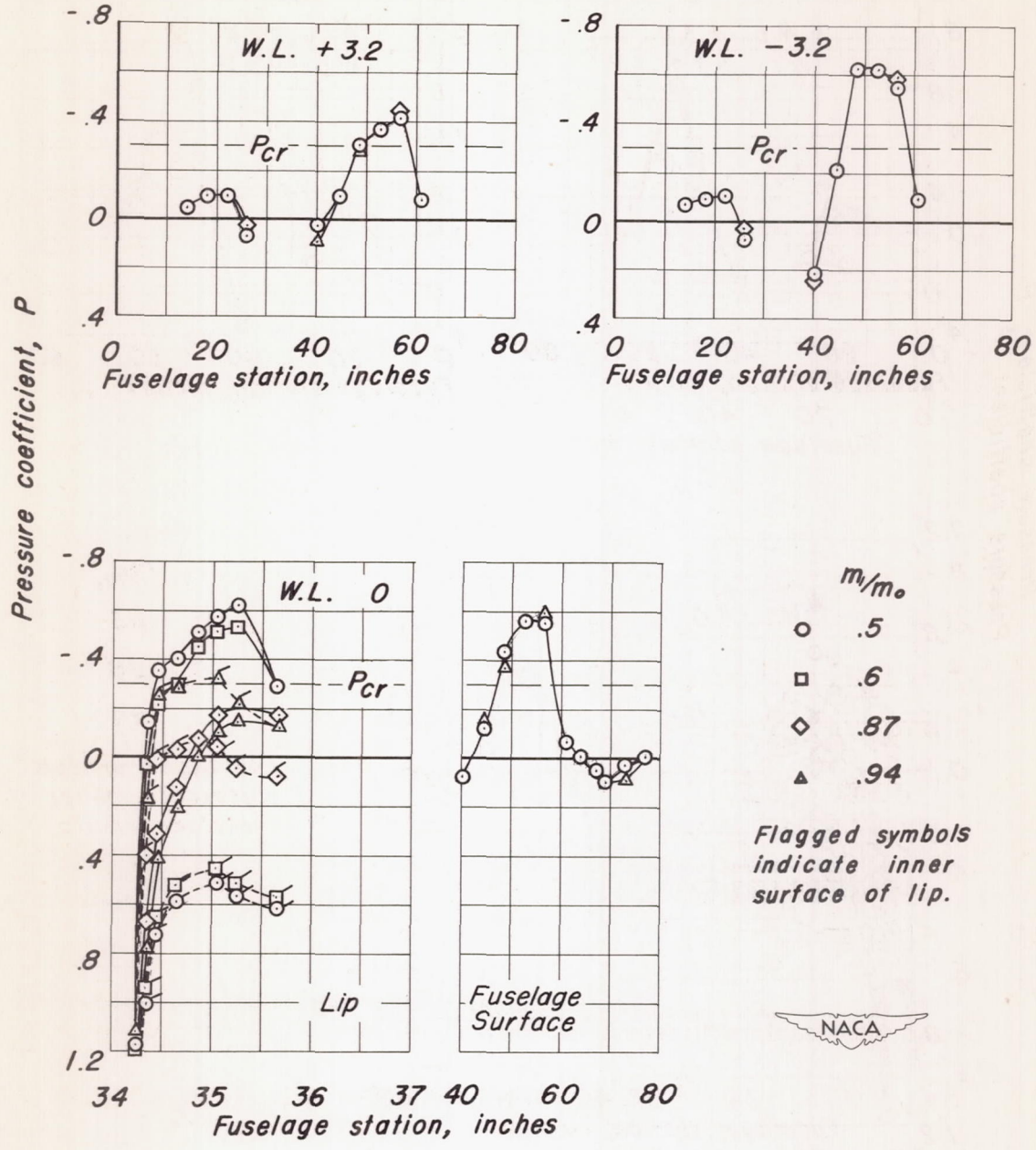

(g) M_0, 0.85; α_u, 0°.

Figure 13. – Continued.

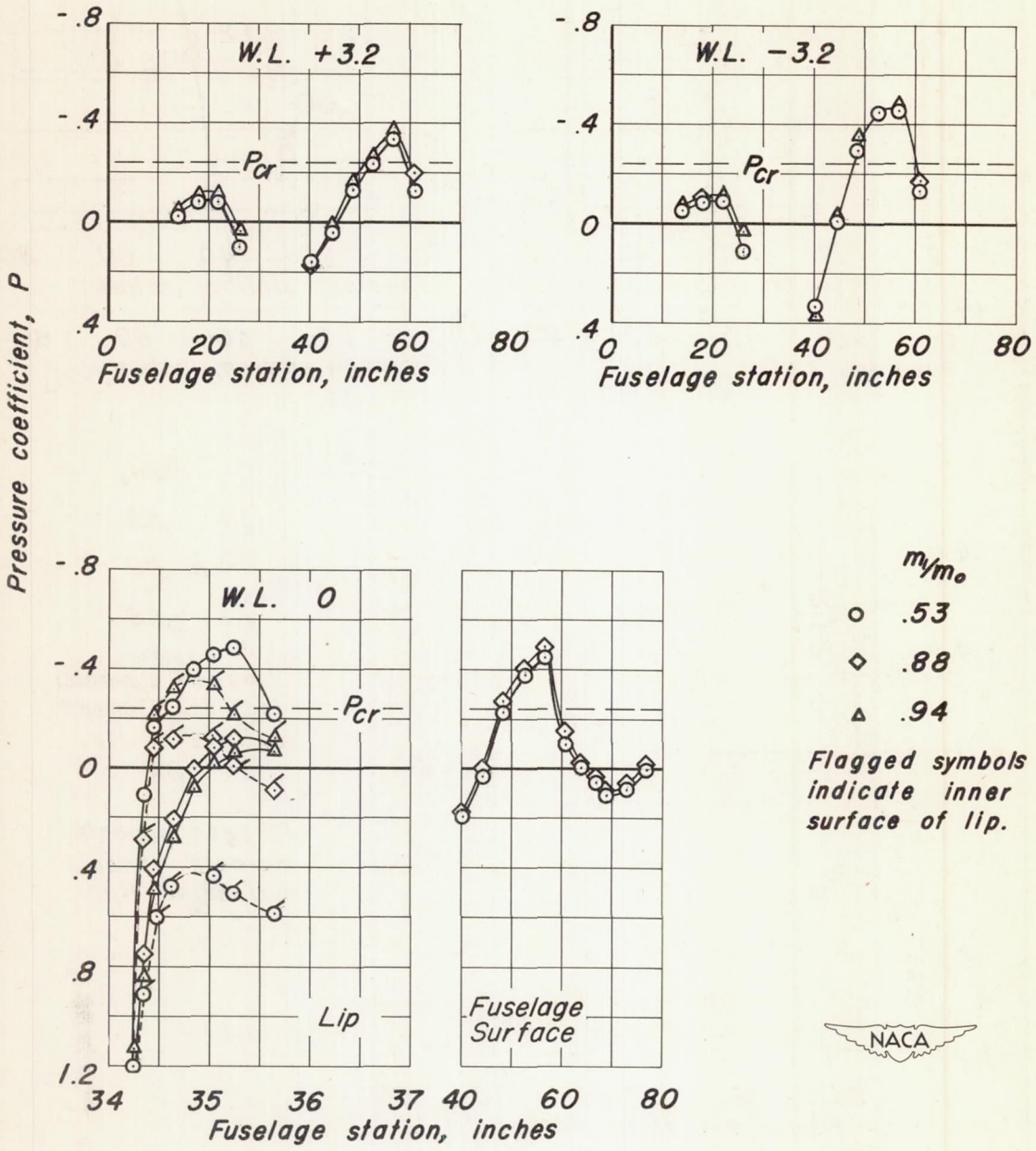

(h) M_o, 0.875; α_u, -2°.

Figure 13. – Continued.

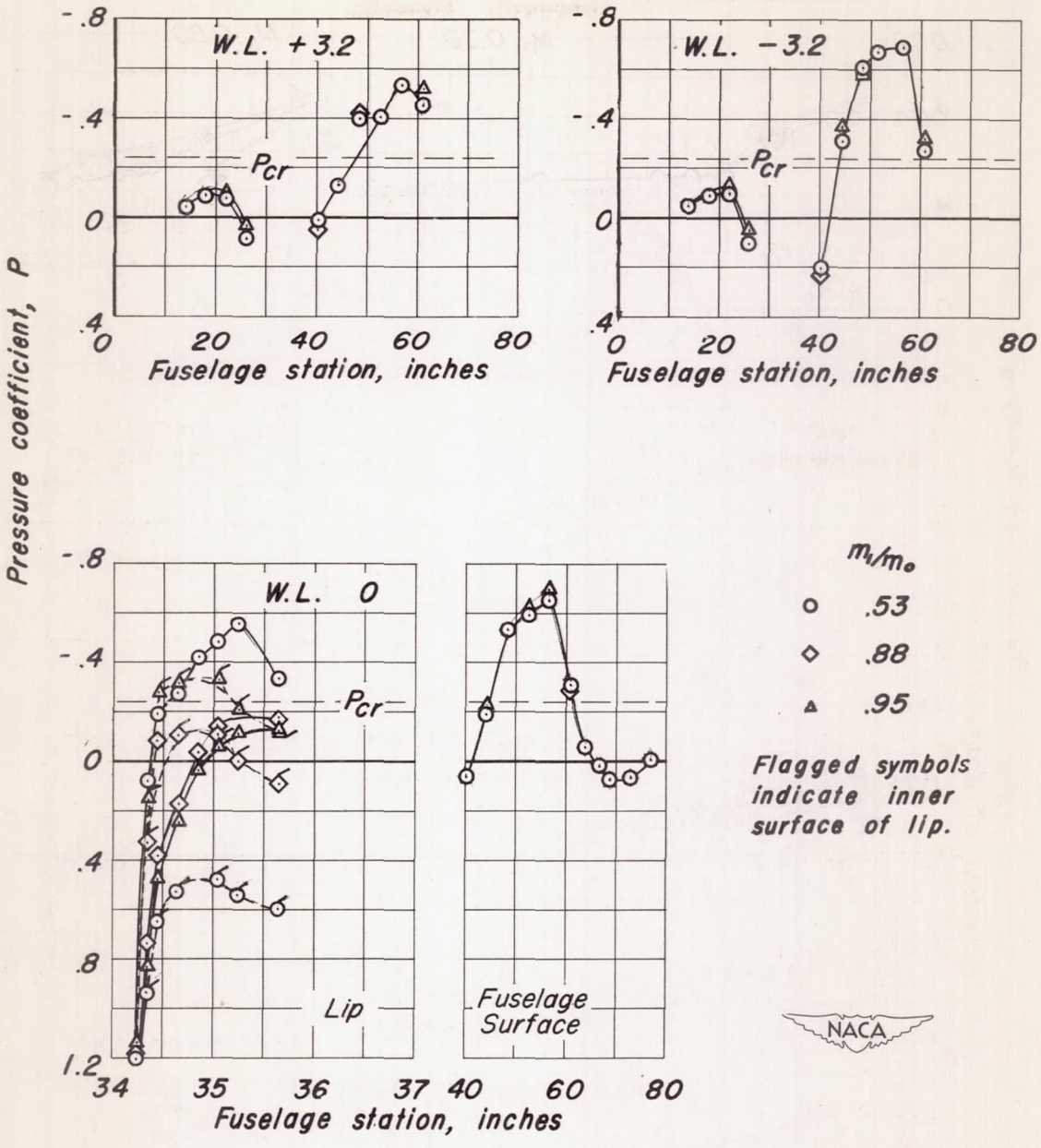

(i) M_0, 0.875; α_u, 1°.

Figure 13. – Concluded.

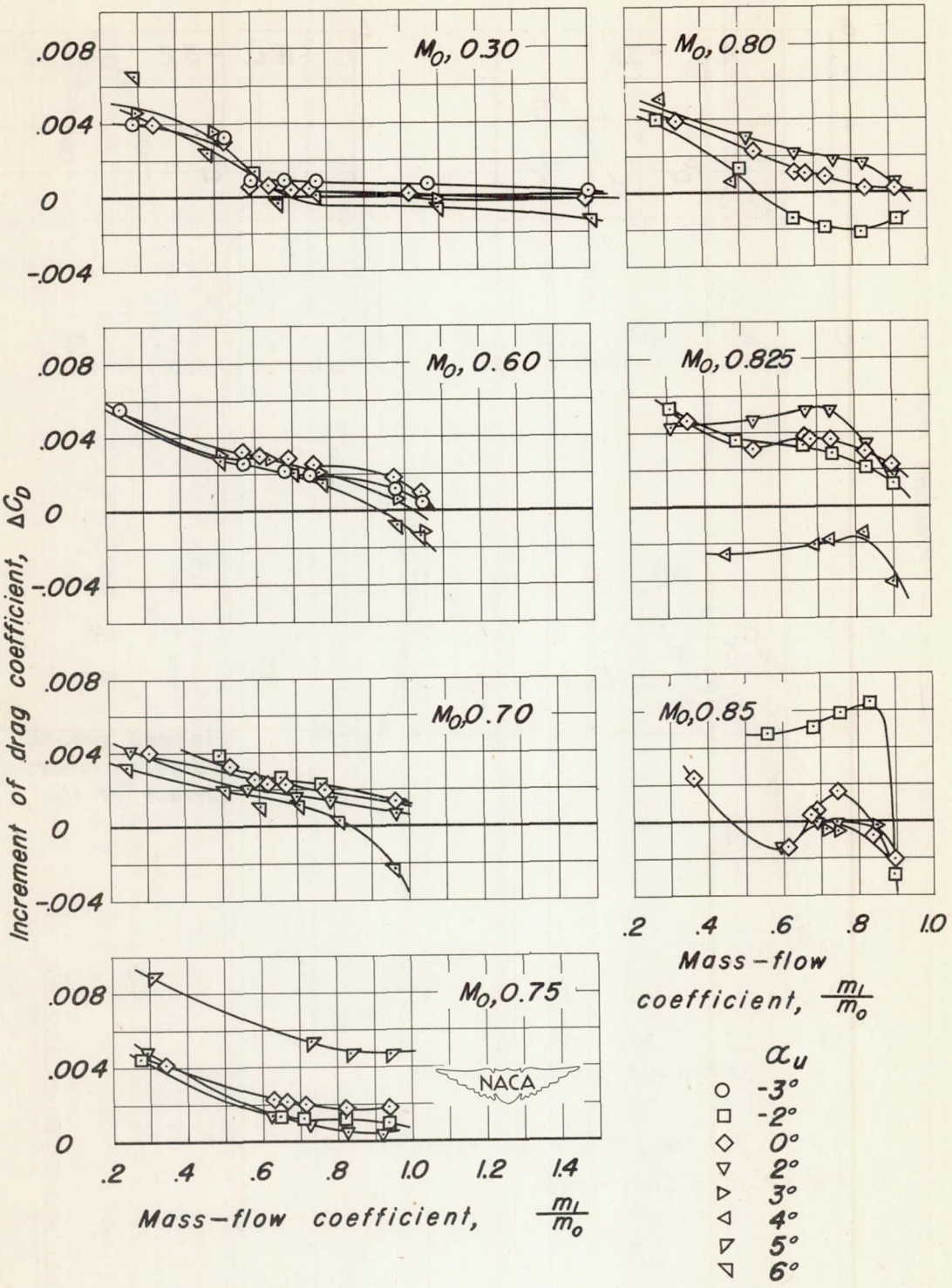

Figure 14.- Increments of drag due to the submerged inlets with deflectors.